Tampere University

Tianqi Lang

DESIGN AND IMPLEMENTATION OF MICROFLUIDIC CHIP TO STUDY CHEMOTACTIC MIGRATION OF CANCER CELLS

Faculty of Automation Engineering
Master of Science Thesis
November 2019

ABSTRACT

Tianqi Lang: Design and implementation of microfluidic chip to study chemotactic migration of cancer cells
Master's thesis
Tampere University
Master's Degree Programme in Automation Engineering
November 2019

Chemotactic movement in response to drug candidates is one of the leading tangible indicators of cell's state, which has widely spread in biomedical fields ranging from normal wound healing to metastatic migration of cancer cells. To facilitate its development, a microfluidic chemotaxis chip has been designed and implemented on top of dynamic cell culture. Different from static chip confining itself to inadequate cellular functions, the microfluidic chemotaxis chip provides a more versatile alternative to enable a better compatible experimental condition forming. A soft lithography-based method is used to prepare chips from polydimethylsiloxane (PDMS), which is a favourable material for manufacturing microfluidic devices. The competitive features of the chemotactic chip include a wide range of controllable flow rates, higher levels of automation, economic feasibility based on the small usage amount of material in microscale, to name but a few. In the chemotactic chip, the mixing efficiency between two inflowing liquids is finely controlled by a syringe or pressure-based pump, resulting in a chemotactic gradient that can be manipulated by adjusting the flow rate. The chip model that applied in the experiments is simulated by COMSOL Multiphysics®, which is a dominated fluidic simulation software. The final selections, such as flow rate, design, and dimension of the chip are contingent on the simulation results and empirical considerations.

Finally, the chip with fluorescein isothiocyanate (FITC) is validated under the microscope. And the experimental data is analysed in comparison to the theoretical data computed from the simulation.

Keywords: Microfluidics, COMSOL Multiphysics®, PDMS, Chemotactic movement, Shear stress

The originality of this thesis has been checked using the Turnitin Originality Check service.

PREFACE

The stage of doing this thesis is almost the last stage of my Master's degree in Automation Engineering. The pending state of the final thesis lasted quite longer than I initially expected. When I started feeling a flurry of frustration after I have received some refuses, I was very fortunate to be taken out of the shell by Prof. Kallio. I can clearly remember as if it were yesterday how excited I was when I received the topic of the final thesis from him. From the bottom of my heart, I do cherish this precious opportunity. Thank him for being more than a supervisor, a professor, for being a kind mentor to me who points out the development direction. I could not go this far without the repeated support of the other supervisor, Joose Kreutzer. The first time I knocked on the office door of Mr. Kreutzer, I still could recall how tense I was. That moment is all very fresh in my mind. I am an ordinary international student like some of them who rarely participate in Finnish social activities, especially the stereotype of Chinese embodies on myself sufficiently. Fortunately, most of my best and happy time of a day was the time I discussed with colleagues or studying in Mr. Kreutzer's office on occasion. His positive attitude to work imperceptibly infects me all the time. He frequently sees the point of my vague ideas and guides me back to correct orientation. Nothing compares to all the knowledge and happiness I harvest in the lab. This period in the laboratory has been an unforgettable experience of my career, for which I will be eternally grateful.

Apart from being 'unlucky' to have no idea about Finnish or fluent English, I have been fortunate in almost every respect in the course of lab time. None of this final thesis would be possible without the support of this remarkable team. The supports from Antti, Anne, Heimo, Jari, Kaisa, Lassi, Matias, and William not only regards to studies but also in every aspect of life. I am pretty sure that I could relatively articulate my thoughts in English than those days back to a year ago because of a bunch of outstanding colleagues along with me. The research group is a wonderful place filled overwhelmingly by people who are motivated by their notion of the scientific interest, by their perception of the public good and by their duty not as researchers, but as representatives to what they believe is right for this country, Finland. As far as I have comprehended from the lab, the principle of our lab is not to be afraid of controversial issues.

In the end, thanks to my father for what he has been sacrificing to me. Thanks to my mother and grandmother for blessing me in heaven.

Tampere, November 4th,2019

Tianqi Lang

CONTENTS

LIST OF FIGURES

LIST OF SYMBOLS AND ABBREVIATIONS

CAD	Computer-Aided Design
CFD	Computational fluid dynamics
CXCL12	C-X-C motif chemokine 12
CXCR4	C-X-C chemokine receptor type 4
DIC	Differential Interference Contrast
DI-water	De-Ionized water
FDM	Finite Difference Method
FEM	Finite Element Method
FITC	Fluorescein Isothiocyanate
FVM	Finite Volume Method
HNA	HF/Nitric/Acetic Acid
ITO	Indium Tin Oxide
KOH	Potassium Hydroxide
LOC	Lab-on-a-Chip
MEMS	Microelectromechanical Systems
ME	Mixing Efficiency
NS	Navier-Stokes
PARDISO	Parallel Direct Sparse Solver Interface
PDEs	Partial Differential Equations
PDMS	Polydimethylsiloxane
PVP	Polyvinylpyrrolidone
RF	Radiofrequency
SAV	Area-to-Volume
SDF-1	Stromal cell-derived factor 1
SLAS	Society for Laboratory Automation and Screening

a	Circle radius
A	Cross-section area
β	Viscosity ratio
C	Speed of sound
c	Concentration of a chemical
C_p	Specific heat
D	Diffusion coefficient
D_h	Hydraulic diameter
d	Relevant mixing path
E	Electrical force vector
F	Force
g	Gravitational force vector
h	Height of the channel
l	The position within the height of the microchannel
Kn	Knudsen number
k	Conduction coefficient
k_B	Boltzmann constant
L	Length of the channel
Lp	Physical length scale
Ma	Mach number
N_A	*Avogadro constant*
P	Pressure
Pe	Péclet number
P_{el}	Charge density
P_{wet}	Wetted perimeter
Q	*Volumetric flow rate*

q	Thermal energy
Re	Reynolds number
T	Temperature
t	Diffusion time
τ	Wall shear stress
U	Velocity magnitude
v	Flow velocity
ρ	Density
η	Viscosity
λ	Molecular mean free path length
∇	Gradient

1. INTRODUCTION

Richard Feynman's speech [1] – "there is plenty of room at the bottom" - opened the minds of researchers and companies to the possibility of exploring the potential of microstructures of precise dimensions. The development of microelectromechanical systems (MEMS) and the megatrend of minimizing the size to achieve economic feasibility of mass production have resulted in substantial new applications and researches to the list of top topics over the last 30 years. Microfluidics is one branch of MEMS that started appearing an appealing economic and research potential since George Whitesides [2] and Steve Quake [3] published papers about polydimethylsiloxane (PDMS) microfluidics and soft lithography respectively in 1999 and 2000. New fabrication methods related to PDMS and photolithography enable creative possibilities in terms of biomedical or chemical researches that were not previously possible. This thesis is established based on the fundamentals and development of microfluidics, which aims to generate a steady and compatible circumstance within the microfluidic chip for preliminarily analysing cell's chemotactic movement and then for validating the efficacy of drug candidates. The trend of chemotactic migration is a remarkable characteristic of cancer cells, which reflects whether cells are favourable to live in a circumstance or not [4] [5]. In this thesis, a controllable chemotactic gradient achieved by regulating flow rate is employed to study the cell’s chemotactic movement. Theoretically, the requirement of the desired gradient is to minimize its mixing efficiency to meet the biomedical objectives. However, considering a collection of constraints, such as the limited magnitude of shear stress, merely thinking by way of increasing flow rate to minimize diffusion efficiency is insufficient. The corroborative discussion is illustrated in the following chapters.

This thesis is a part of the collaborated project between Tampere University and University of Turku, which is mainly intended to design and to implement the chemotactic chip instead of studying cell migration. Theoretically, the thesis aims to develop a stable microfluidic platform that enables four chips to work simultaneously for 24 hours. The biomedical part of the research is mentioned briefly as needed to improve the integrity and consistency of the thesis.

The structure of this thesis is presented in a list as follows: In Chapter 2, the discussion has revolved particularly around a collective of technical terms concerning the background of this thesis – microfluidics, and chemotaxis. In Chapter 3, the material and method implemented have been illustrated in chronological order, ranging from the chemotactic chip design to assemble the microfluidic platforms. In Chapter 4, the data

from experimental validations and simulation has been comprehensively analysed in different aspects. The conclusion is presented in Chapter 5.

2. THEORETICAL BACKGROUND

2.1 Lab-on-a-chip

A biomedical analysis is essential to the development of contemporary biology, chemistry, and medicine. The traditional way of biomedical analysis is often staged on a large workbench where biomedical samples are handled with various operations - separation, mix, filtration, purification, reaction. As the development of biomedical analysis over the years, a miniaturized system, Lab-on-a-chip (LOC), is widely used because of its high efficiency and low cost. The principal of LOC is to aim to integrate all operational functions that used to be manipulated in a traditional workbench to a micro or nano-scale chip. Theoretically, LOC contains a series of inter-discipline knowledge ranging from fluidics, MEMS, chemical analysis, and biology. Its development is based on biomedical analysis, the method of micro-fabrication technology, and the structural feature of a network of microfluidic channels. [6] In 1985, the first LOC device, a microfluidic device was designed for detecting pregnancy by Unipath corporation [7]. Due to its first commercial success, various applications emerge one after another. For instance, by the middle 1990s, the chips based on microarrays and microfluidics have stepped in the substantive stage of commodity development. Ciba-Geigy, Alberta University, Oak Ridge National Laboratory, University of California of Berkeley, and PerSeptive Biosystems successively reported the achievement of analysing systems based on an integration of integrated electric power drive, microfluidic channels and separation system [6].

The motivations pushing the development of microfluidic chips are not only a high degree of automation, integration, economic efficiency, and high throughput but also some ethical considerations. The microfluidic chip was applied to establish an *in vitro* model of organs for drug testing in the wake of the principle of "the three Rs" (reduction, refinement, and replacement) associated with the use of experimental animals was attached importance by society [8]. As the outcry provoked by animal protection institutes becomes intense, the utilization and development of LOC started to emerge high commercial and ethical values in terms of drug discovery. Except for its well-known advantages, like portability or economic feasibility, its ability to mimic cellular circumstances, including cell-cell interaction, oxygen concentration, or circulatory flow, is more significant. Some outstanding applications, for example, a microfluidic device generating perpendicular chemical and oxygen gradients for drug research [9], or achieving electroporation for delivering drugs into cells within a lab-on-chips device [10], sufficiently appears that LOC

has many potential applications for drug research. In conclusion, LOC draws a more efficacy and safety way to test drugs in clinical trials or scientific experiments.

2.1.1 Cell-based drug development

Cell-based drug development plays a critical role in the methods of drug discovery. The screening drug based on several cells' behaviours in response to drug candidates has widely used because people has expressed an ethical consideration of testing drugs on animals from 20 years ago [8]. One of the most common cell-based methods of validating the functions of a potential drug is imaging and analysing the relationship between cells' activity and drug candidate within a static petri dish regularly. It displays the advantages combined the high throughput and effortless operability. However, considering the concerns that the lengthy process of drug research, the exorbitant cost to research, and the low capability of the static cultures predicting the performance of the drug, a way of microfluidics-based drug research started entering scientist's view.

The utilization of microfluidics-based drug research has several advantages, making it a promising alternative to conventional drug research methods. It is a reliable *in vitro* device as an alternative to conventional *in vivo* investigations [11]. One of its advantages makes compelling progress in terms of mimicking the circumstance that bloodstream is flowing in the vessels. This advance encourages a big step forward to the final goal that achieves to mimic a sophisticated metabolic system *in vitro*. The more physical and chemical variables of the metabolic system *in vivo* that can be manipulated *in vitro*, the more corroborative measurements will be. Another dominated advantage of microfluidics research is saving the investment cost from the reduction of the usage volume of drug candidates. Most often, the drug candidates are exceedingly costly. Considering the microfluidics market was valued at $1.6 billion in 2013 [12], let alone the investment devoted to traditional ways of drug discovery.

Furthermore, a controllable microfluidic device could provide support for generating expected experimental microenvironments, like linear or nonlinear concentration gradient [13] [14]. These concentration gradients are essential to the high-throughput study of cell-based drug development [15]. This thesis is mainly expanded on top of the way of implementing this gradient on drug development.

2.1.2 Chemotactic movement

Chemotaxis is a remarkable characteristic of cells induced by chemokine, which is a family of signal proteins. Chemokines target a family of protein-coupled receptors (GPCRs), which results in a directed motion of cells [16]. This directed motion is called

chemotactic movement, which is a concrete reaction derived from chemotaxis. Chemotactic movement is used by white blood cells to combat infections, by embryonic cells to form tissue patterns, and by cancer cells during metastasis. Particularly in terms of cancer cell, the CXC chemokine stromal cell-derived factor-1 (SDF-1, also known as CXCL12) and its receptor, C-X-C chemokine receptor type 4 (CXCR4) guide cancer cell's metastasis in a human body which is fatal to a cancer patient [17]. Cancer cells favour the area with a high concentration of chemokine, which results in cancer metastasis. Taking advantage of this phenomenon, whether a drug candidate is valid or not can be judged by the chemotactic movement of cancer cells. If the cancer cells still move forward to high concentration areas after drug treatment, this drug candidate tends to be invalid. Because it does not inhibit the effect of CXCR4 and CXCL12, which guides cancer cells to an 'easeful area'. Vice versa.

2.1.3 Chemotactic gradient

As the study of chemotactic movement has become progressively mature, it is much harder to satisfy researchers' demanding requirements. Thus, the intention of controlling chemotactic movements was proposed [18]. Some scientists put forward that a way of directly managing chemotactic gradient appeared to have a prominent potential to control chemotactic movement indirectly. Figure 1 is a schematic diagram illustrating the definition of chemotactic gradient.

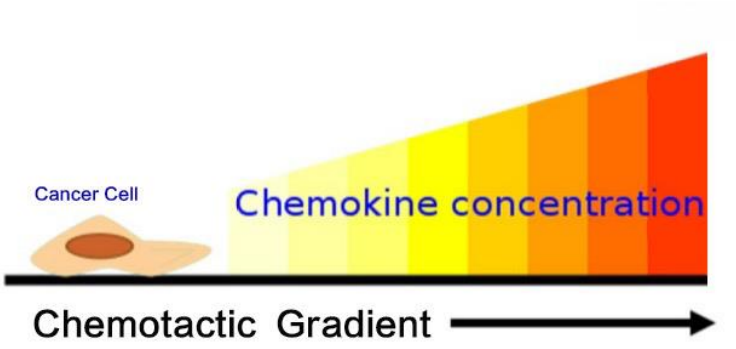

Figure 1. *The schematic diagram of chemotactic gradient*

Because cancer cells exhibit an ability to sense concentration chemokine that directs their motions. The direction of chemotactic movement of cancer cells is along the chemotactic gradient. Thus, the way of controlling chemotactic gradient is widely studied in recent years.

Until now, some instrumental methods have been put forward to create desired gradients of chemotactic reagents. By way of illustration, one of the earliest methods of leukocyte

chemotaxis studies using agarose and collagen gels fares adequately [19] [20] [21]. The method of agarose or collagen facilitates to get a pattern of the chemotactic gradient utilizing the diffusion of chemokine through the gel. Meanwhile, some non-gel techniques, like the Zigmond chamber or the Dunn chamber, express its profound values to some extent as well [22] [23]. The Dunn chamber set the stage for generating a chemotactic gradient by the diffusion over a short distance between two fluid-filled reservoirs. Different technology has a different propensity for achieving a chemotactic gradient. However, each technique will appear in its inadequate aspects sooner or later as the demands of the market turn to be more diversified.

In summary, there are three main functions that the methods as mentioned earlier couldn't match properly, including the need for a pattern of an arbitrary gradient, a feasible way of changing the chemokines or solutions in mid-experiment, and a virtually changeless and stable gradient over experimental time. Employing the approach of involving agarose and collagen is not capable of acquiring arbitrary pattern of chemotactic gradients except linear ones, which rely on the diffusion merely. The definition and property of diffusion is illustrated in Section 2.2.5. Besides, the shape of the gradient created within the gel varies from time to time until it ends up to the saturation level. This high degree of dynamic change brings adverse effects to the research of cell migration to a varying degree. Furthermore, considering the situation that the chemotactic gradient *in vivo* might increase or decrease without a regular order as a function of distance in vessels, the prior techniques leave a lot to be desired. Besides, in the time of scientists require to change the species of chemokines during the experiment for acquiring a series of comparable data, these prior methods don't appear an ability to achieve.

The more controlled parameters are manipulated, the more accurate data are embraced. Microfluidic tools could be one of the ideal solutions to control the chemotactic gradient because of its versatility and compatibility. The microfabrication method facilitates to achieve arbitrary chemotactic gradients (i.e., linear, ramp, parabolic) for microfluidic devices [24]. Figure 2 illustrates how different network and different flow rate influence the chemotactic gradients.

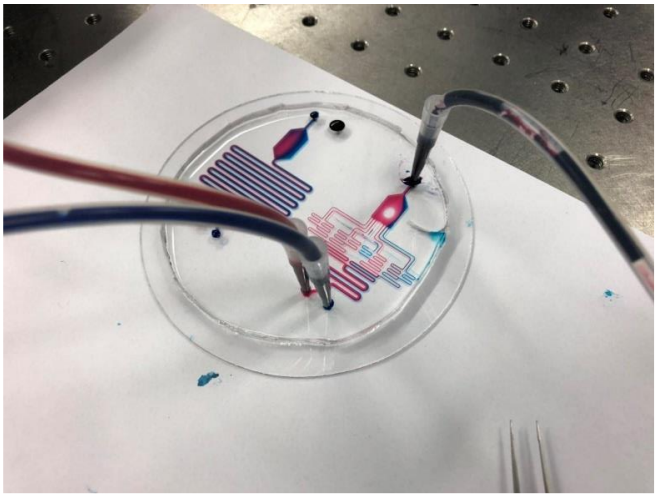

Figure 2. *Two different networks of channels*

The various networks of channels accompanying with various flow rates enable the chemotactic gradients to be more controllable and submissive. Besides generating arbitrary patterns of a chemotactic gradient, the microfluidic tool can maintain the constant shape of a chemotactic gradient over a long period as well. The status of the chemotactic gradient is approximately like a changeless status on condition that the flow rate is constant. Furthermore, the intention of changing chemokine or solution in the mid-experiment can be effortlessly achieved by switching to a reservoir of targeted chemokine solution during the experiment. The microfluidic tool enables creative possibilities that weren't previously possible.

The objective chemotactic gradients in this thesis are two different linear chemotactic gradients (ideally fully-developed mixing or ideally non-mixing), which are created to study a set of comparative experiments, one is involved with drug-treated cells and the other not. By way of illustration in Figure 3 and Figure 4, assume that the inflowing liquids represent chemokine-free (white) and chemokine-rich (orange) cell growth medium. The chemotactic gradient generated from two liquids is dependent on the amount of the corresponding magnitude of flow rate. As a high-throughput method of developing drug research discussed in Section 2.1.2, studying chemotactic movement of cancer cells can support a shred of strong evidence to validate the effectivity of a drug candidate. Figure 3 represents the hypothetical chemotactic movement of drug-treated cancer cells and non-treated cancer cells in response to an ideally fully-developed mixing chemotactic gradient. The ideally fully-developed mixing gradient refers to the concentration of chemokine (orange) changes along the length of the channel from beginning 100% to end 50%.

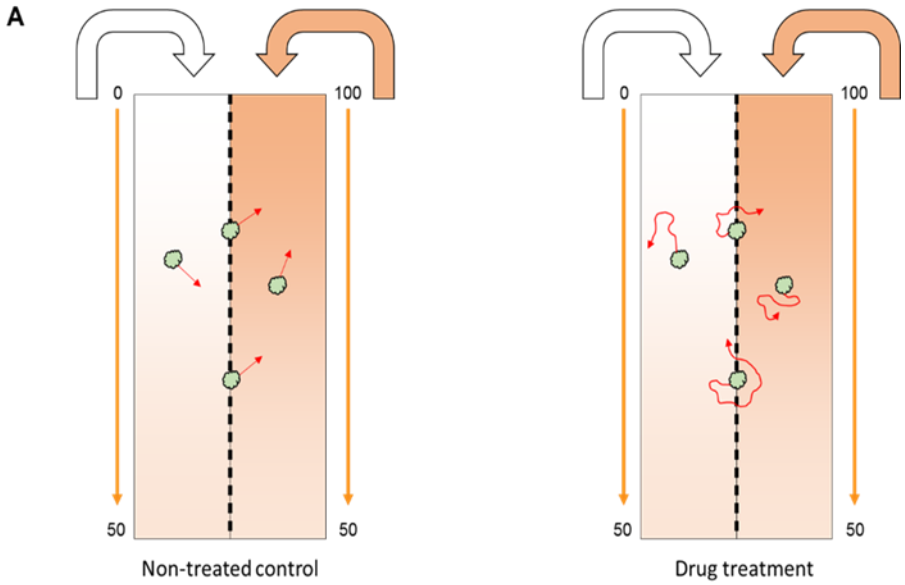

Figure 3. *Chemotactic movement of non-treated cancer cells (left) and drug-treated cancer cells (right) in the fully-developed mixing gradient*

Based on the effect of chemotaxis on cancer cells, the chemotactic movement of non-drug-treated cancer cells is a directed motion to the chemokine-rich areas along the chemotactic gradient where it is supposed to be the zone of the top right corner in this case. Whereas, the chemotactic movement of drug-treated cancer cells shows an unpredictable and irregular pattern. Because drug candidates may compromise cancer cell's chemotactic sense, and cancer cell's ability for directed migration will be reduced. Thus, merely depending on the unclear trajectory of drug-treated cancer cells to judge the efficacy of a drug candidate is ambiguous.

In consideration of the preceding insufficiency, the other chemotactic gradient is applied to make cancer cell's chemotactic movement clear. In contrast to the former chemotactic gradient, this one aims to do best to approach the status of ideal non-mixing. The ideal non-mixing gradient refers to that the concentration of chemokine (orange) keeps 100% along the length of the channel, regardless of the effect of diffusion (see Figure 4). Under higher pressures, at which the two liquids do not mix, cancer cell migration is expected to be random until a cell reaches the central verge at which the two liquids meet. There is no doubt that non-treated cancer cells will move to the chemokine-rich side. However, for drug-treated cancer cells, they favour the chemokine-rich side, unless their chemotactic sensing has been compromised by drug treatment. Instead of monitoring and analysing the complicated trajectory of chemotactic movement in the preceding method, merely observing the last location of drug-treated cancer cells (located in the white or orange area) can validate the efficacy of a drug candidate.

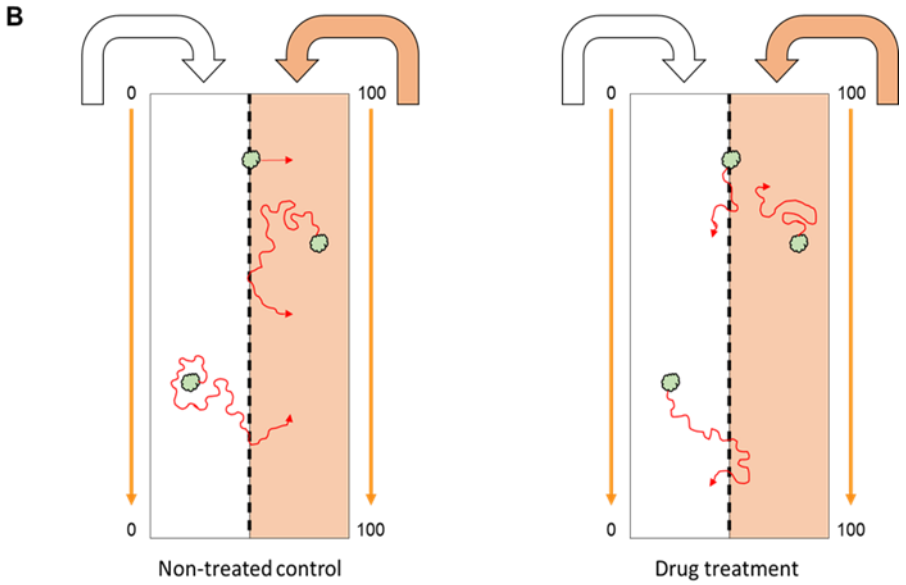

Figure 4. *Chemotactic movement of non-treated cancer cells (left) and drug-treated cancer cells (right) in the non-mixing gradient*

2.2 Fluid principles

Fluid, as one of the main objects studying in the field of LOC, is widely applied because of its two leading characteristics – small dimension and versatile function. Some characteristics of the fluid in the microscale are distinguishing from macro-scaled counterparts, which enable creative functions that weren't previously possible. Taking advantage of these characteristics, LOC could implement more functions and applicants, for example, chromatographic chip or micromixer [25]. In this section, some behaviours of fluid will be illustrated in different scales.

2.2.1 Navier-Stokes equations

It is common knowledge that three laws of motion enable a movement to be expressed in the way of classical mathematical expressions in the macroscopic world. It is inevitable to discuss and reference Navier-Stokes (NS) equations in a fluid study, which have the same dominate status in fluid mechanics as three laws of motion in classical physics.

NS equations as one of the most versatile mathematically ways to model liquid flow are established on three primary conservation laws of thermodynamics, *mass conservation*, *momentum conservation*, and *energy conservation*. Considering the fluid flow is subjected to density (ρ), viscosity (η), pressure (P), flow velocity (v), specific heat (C_p), and temperature (T), the NS equations is expressed in the way of involving these parameters.

The first equation is *mass conservation* which is presented as:

$$d_t\rho + \rho\nabla \cdot v = 0, \tag{1}$$

where,

$$d_t = \frac{\partial}{\partial t} + v_x\frac{\partial}{\partial x} + v_y\frac{\partial}{\partial y} + v_z\frac{\partial}{\partial z}, \text{ and } \nabla = \frac{\partial}{\partial x} + \frac{\partial}{\partial y} + \frac{\partial}{\partial z} \tag{2}$$

Assume v_x, v_y, v_z are velocity components in the Cartesian coordinate system (*x, y, z*). For incompressible fluids, the density is constant. Thus, this equation is simplified to:

$$\rho\nabla \cdot v = 0 \tag{3}$$

The second equation is *momentum conservation*. Momentum can change by convection or flux through the surface of a unit volume and by the action of forces. Typically, the forces include surface forces, i.e., pressure forces and viscous forces, and external body forces, e.g., gravitational and electric forces.

$$\rho(\partial_t v + (v \cdot \nabla)v) = -\nabla_p + \eta\nabla^2 v + \beta\eta\nabla(\nabla \cdot v) + \rho g + \rho_{el}E, \tag{4}$$

where β denotes viscosity ratio, g refers to the gravitational force vector, P_{el} means charge density, and E means electrical force vector.

For incompressible fluids, the equation is simplified as:

$$\rho(\partial_t v + (v \cdot \nabla)v) = -\nabla_p + \eta\nabla^2 v + \rho g + \rho_{el}E \tag{5}$$

Typically, the microscale fluid corresponds to incompressible flow in most applications. To validate the fluid applied in this thesis is an incompressible flow, Mach number (*Ma*), a dimensionless quantity representing the ratio of velocity (v) of a fluid past a boundary to the speed of sound (C) in that fluid will be referenced.

$$M_a = \frac{v}{C} \tag{6}$$

The premise of referencing the NS simplified equations is liquid flow is incompressible, resulting from its *Ma* is less than 0.3. In the thesis, the dimension of flow rate is in micro-liters per minute, the dimension of the cross-section of the channel is in square micron, and the dimension of the speed of sound is in meters per second. The value of *Ma* is far less than 0.3, so it is an incompressible flow.

The third equation is *energy conservation*.

$$\rho C_p\left(\frac{\partial T}{\partial t} + v_x\frac{\partial T}{\partial x} + v_y\frac{\partial T}{\partial y} + v_z\frac{\partial T}{\partial z}\right) = \frac{\partial}{\partial x}\left(k\frac{\partial T}{\partial x}\right) + \frac{\partial}{\partial y}\left(k\frac{\partial T}{\partial y}\right) + \frac{\partial}{\partial z}\left(k\frac{\partial T}{\partial z}\right) + q, \tag{7}$$

where k denotes conduction coefficient, and q means the thermal energy generated by a source or removed from sink.

2.2.2 Scaling effect

NS equations are veritable mathematical laws in an assortment of fluidic researches. However, some definitions and formulas related to classic fluid dynamics in macro-level need to be restudied in the microscale.

Microfluidics, as a branch of MEMS, inherits most characteristics of MEMS, including micro miniaturization, batch production, integration, to name but a few. In addition to those characteristics, the scaling effect is a leading characteristic when microscale fluid is involved. The scaling effect exists extensively in nature, which is not only confined in the field of microfluidics. In the macro world, gravity is a ubiquity of force in daily routines. The gravity of the fluid is a more dominated force to determine the state of fluid than capillary force, electrostatic force, or Van der Waals Force. However, when scaling down the dimension of an object, some kinds of relatively significant forces in macroworld do not keep the same weighted importance in the microworld. The shift in dominance between different phenomena as the dimensions of the system change [25]. More specifically, inertial force or electromagnetic force is proportional to the higher order of characteristic size as it decreases. Whereas, viscous force, elastic force, surface force, and electrostatic force are proportional to the lower order of characteristic size as it increases. In some circumstances, the scaling effect could flip the dominance of forces upside down.

By way of illustration, assume that a cubic "drop" of water's length of a side is 1 m. The area of this cube unquestionably equals the squared of its edge length 1 m^2, and volume would have the dimension of length to the power three, 1 m^3. Provided that 1 m will decrease to one-tenth of its original length, 0.1 m, it is evident that the degree of change in terms of volume is more than that of an area. Furthermore, the surface area-to-volume (SAV) ratio will increase from 1 m^{-1} to 10 m^{-1} and thus renders any surface phenomenon tend to become more dominant than the volume factor as dimension decreases [26]. According to some empirical studies, in the case of the value of SAV of fluid is less than 1, the characteristics of this fluid are consistent with macroscopic fluid. The NS equations are still capable of demonstrating the characteristics of microscale fluid on condition that the continuum assumption. The assumptions of fluid are incompressible, and no-slip at the fluid-solid interface could stand as well. Whereas, if the value is far more than 10^6 m^{-1}, the surface force turns to be the dominated factor affecting fluid properties. Hence, such assumptions like continuum assumption, the compressibility of fluid, viscous dissipation, slip flow, temperature jump, and intermolecular force need to be redefined utiliz-

ing *mass conservation*, *momentum conservation*, and *energy conservation*. For instance, NS equations are deficient to be applied in the case of the dimension is as small as the mean free path of molecular because the continuum assumption is not valid.

2.2.3 Boundary conditions

Fluid mechanics has three basic equations: the continuity equation based on the principle of mass conservation, the momentum equation based on the principle of momentum conservation and the energy equation based on the principle of energy conservation. Whether these equations are valid under the microscale conditions or not are subject to the selected scale and its corresponding ambient factors.

In general, the "no-slip" and "incompressible" conditions derived from the momentum equation and the "no temperature jump" condition derived from in energy equation are widely embraced in microfluidic applications. However, in a strict sense, these boundary conditions can only be applied if the flow near the wall is in thermodynamic equilibrium resulting from a theoretically exceedingly high collision frequency between the fluid and the solid surface. Practically, that ideal high collision frequency could not be implemented so that a slip in the direction of tangential velocity and the effect of temperature jump exists in every microfluidic device in varying degrees.

In an aim to reference the mathematically fluidic expressions accurately to solve various dimensional flow questions, Knudsen number (*Kn*), a dimensionless number defined as the ratio of the molecular mean free path length (λ) to a representative physical length scale (*Lp*) is introduced.

$$\mathrm{K_n} = \frac{\lambda}{\mathrm{Lp}} \tag{8}$$

Depending on the value, *Kn* is defined and categorized by different laws and equations (See Figure 5). By way of illustration, in the case of *Kn* trends to 0, the fluid is supposed to express by Euler's equation. If *Kn* trends to 0.001, the fluid is fitter for the NS equations of the "No-slip" boundary condition. At this point, the fluid is regarded as a continuous flow. When the value of *Kn* is fall in between 0.1 and 0.001, the fluid is expected to express by the NS equations with the "slip" boundary condition. Considering the condition that *Kn* is over 10, Boltzmann equation is more instructive. In this thesis, the initial profile of microchannel is a rectangle (300 μm * 500 μm), and the expected flow rate is in a range of 1 μl/min to 20 μl/min. Thus, the value of *Kn* trends to 0.001, which refers to conditions like, "no-slip," "incompressible," "no temperature jump," and "continuous assumption" is applied in this thesis.

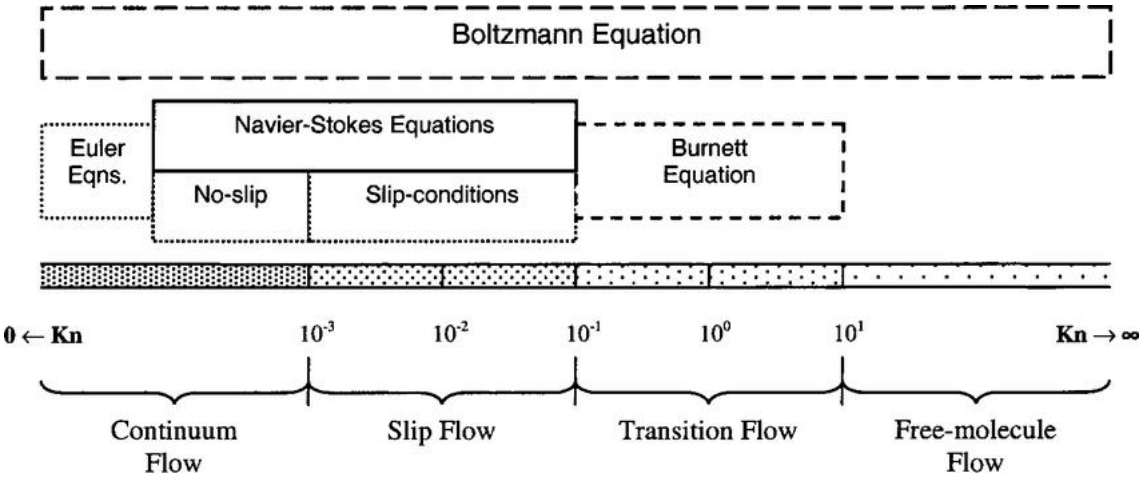

Figure 5. *A range of Knudsen number (Kn) [27]*

2.2.4 Flow type

The premise of developing the values of microscale fluid is to understand its properties and characteristics explicitly. To define a fluid is whether in the range of microscale or not, a non-dimensional number in fluid mechanics, Reynolds number (*Re*) will be introduced that could help to judge flow patterns in different fluid flow situations. Reynolds number is determined as the ratio between inertia and viscous forces.

$$R_e = \frac{\rho v D_h}{\eta}, \tag{9}$$

where D_h denotes hydraulic diameter, ρ refers to density, η refers to viscosity, and flow v means velocity, respectively.

Moreover, the hydraulic diameter of a channel is given as:

$$D_h = \frac{4A}{P_{wet}}, \tag{10}$$

where P_{wet} means wetted perimeter, and A refers to the cross-section area.

Depending on the value of *Re*, the flow regimes are categorized into three types, laminar, transient, and turbulent. The laminar flow is defined that *Re* is in the range of less than 2000. Whereas, transitional flow and turbulent flow result in a range of 2000-4000 and more than 4000 respectively. Laminar flow, the expected flow in this thesis, appears to flow in a manner that fluid elements stay within one layer. Within this flow, the viscous force is more dominated than inertia. Whereas, as the value of *Re* increases, the fluid starts to represent a departure from laminar trend to a turbulent state. At this point, inertia force flips the dominance in dynamic fluid upside down. The fluid is no longer flow within one layer, but instead of flowing in chaos.

By way of illustration associated with this thesis, the solvent is deionized water (DI-water) whose density (ρ) is constant, 1000 kg/m^3. The viscosity of DI-water is 0.001 Pa · s. The velocity is in a range of a minimum of 5.56E-5 m/s and a maximum of 1.11E-3 m/s. Initially, the cross-sectional shape of the channel is rectangular, and its width and height are 1 mm and 300 μm, respectively. Thus, the cross-section area is the product between width and height, 3E-7 m^2. P_{wet} refers to all the perimeters in contact with liquid, which is 2.6E-3 m. Based on the formula above, D_h is 4.62E-4 m. According to the value of all parameters, *Re* is finally calculated to 0.51, which is less than 2000. In conclusion, the type of flow in this thesis is laminar flow.

The different perspectives defining flows have different ways of categorizing. Depends on the driven source, the laminar flow is precisely categorized into Poiseuille flow, and Couette flow further. As the Poiseuille flow, a flow reduced by pressure in straight and rigid channels is the expected flow in this thesis, Couette flow will not be debated. The flow profile of Poiseuille flow seems like a semi-ellipse in which all streamlines flow in a parallel uniformly (see Figure 6). The streamline, which is closer to the infinite, parallel-plate reflects a trend of decreasing velocity, because of the effect of shear stress. More details about shear stress are discussed in Section 2.2.7.

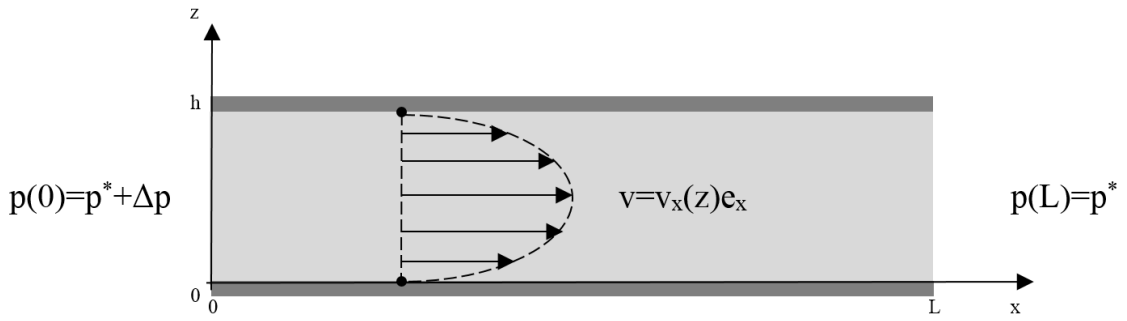

Figure 6. *The flow profile of a Poiseuille flow[28]*

Furthermore, considering the number of different phases flowing in the tubing, microfluid can be categorized into five flow types, which include single-phase microfluid, two-phase microfluid, multiphase microfluid, open microfluidics, droplet microfluidics, and digital microfluidics respectively [25]. Single-phase microfluid as the most usual and studied type of microfluid is an only flow type applied in this thesis theoretically because flow with a single homogeneous phase is the precondition of researching chemotactic gradient. In conclusion, the fluid is single-phase, laminar, Poiseuille flow in this thesis.

2.2.5 Diffusion and mixing efficiency

The research of diffusion and mixing in the microfluidic system is demanding. Pursing a more efficient way to control diffusion always has a tremendous profound value for biomedical analyse. For instance, in a microreactor case, it is necessary to encourage solutes to mix rapidly and effectively and then to accelerate chemical reactions and save the consumption of drugs.

The characteristic scale of fluid is relatively small, and the flowing performance in the microchannels is laminar. Based on the characteristics of laminar flow discussed in Section 2.2.4, the flow profile of laminar flow is a collective of paralleled streamlines in the shape of a parabola. Thus, the mixing between two parallel flows is mainly subjected to the effect of diffusion instead of advection. Comparing to turbulent flow with a high degree of uncertainty in mixing efficiency, laminar flow represents a possibility of controlling mixing efficiency because of its uniform flow profile. In order to explicit, the degree of dominance between the effect of diffusion and effect of advection within a laminar flow, the *convection-diffusion equation*, and *Péclet number* is introduced to convert an intangible phenomenon to a concrete numerical value.

$$\frac{\partial c}{\partial t} = D\nabla^2 c - v \cdot \nabla c, \tag{11}$$

where *c* denotes concentration of a chemical, *D* means diffusion coefficient, as well as ∇ means gradient.

In this form, the convection-diffusion equation combines both parabolic and hyperbolic partial differential equations. The expression, $D\nabla^2 c$ is diffusion term. Whereas, $v \cdot \nabla c$ is the convection term. Furthermore, *Péclet number* represents dominance in the form of a ratio.

$$p_e = \frac{v}{u} = \frac{v \cdot \nabla c}{D\nabla^2 c} = \frac{D_h \cdot U}{D}, \tag{12}$$

where *U* denotes velocity magnitude, D_h means hydraulic diameter.

The Péclet number for mass transport is comparable to the Reynolds number for momentum transport [29].

As discussed before that the effect of convection to mixing is measly in the microscale, researching the factors that influence diffusion are top priorities. According to *Einstein's diffusion law*, the diffusion is determined by a relationship between diffusion time (t), diffusion coefficient (D), and relevant mixing path (d).

$$t = \frac{d^2}{2D} \tag{13}$$

From the perspective of microscopic particles, diffusion refers to the random movement of particles in a certain region under *Brownian motion*, which eventually makes the average concentration of particles in the whole region constant. The diffusion coefficient (*D*) is a direct result of Brownian motion, which is subjected to the particle radius (*a*), temperature (*T*), and some constants, including Avogadro constant (N_A), Boltzmann constant (k_B), viscosity (η).

$$D = \frac{\mathrm{k_B T}}{6\pi\eta a} \tag{14}$$

Thus, adjusting the diffusion coefficient to control diffusivity would not stand up to scrutiny. Then when it comes to diffusion time through a certain length of mixing path, it is determined by the flow rate (product of flow velocity and the area of the cross-sectional profile) applied in a microchannel. It is evident that the bigger flow rate, the shorter diffusion time. The last factor, the length of the mixing path, is in a direct proportion to diffusion as well.

Furthermore, in order to define a degree of mixing under the effect of diffusion and convection at any cut planes in a channel, a prevalent mixing efficiency formula is referenced in this thesis [30].

$$S = 1 - \frac{\left(\int_{A_x} |C_x - C_\infty| \, dA_x\right)/A_x}{\left(\int_{A_i} |C_i - C_\infty| \, dA_i\right)/A_i} \tag{15}$$

Where *x* refers to *x*- cut plane, which can be any cross-sectional cut planes selected in a channel. The symbol *c* denotes concentration profile of species across the channel, and *A* refers to area of cross-sectional plane. The symbol '*i*' refers to the cut plane in the unmixed concentration. Besides, ∞ is ideally considered as the cut plane at infinity, which refers to a fully-developed mixing status. Some other mixing efficiency formulas using the ratio of standard deviation value or the ratio of squared value can also stand up to scrutiny [28] [31].

$$S = 1 - \frac{\left(\int_{A_x} (c_x - c_\infty)^2 \, dA_x\right)/A_x}{\left(\int_{A_i} (C_i - C_\infty)^2 \, dA_i\right)/A_i} \tag{16}$$

However, standard deviation is a number often used to reflect the degree of discretization in a set of data. Moreover, squared value is often used when the difference between two random data out of a set can be either negative or positive. In this thesis, in order to study a more straightforward difference between real data, the mixing efficiency with absolute value is employed.

2.2.6 Micromixer

As the study of mixing efficiency and network of microfluidic channel continues to develop in fast speed, more and more articles prefer to categorize this study as the study of micromixer.

In summary, there are three fundamental motivations of researching micromixer, which are:

1. To expedite mixing, for example, the reactants are enhanced to mix rapidly and sufficiently in a short time within micromixer.
2. To slow down or separate mixing, for example, separating different particles based on centrifugal force or minimizing mixing efficiency, like the micromixer in this thesis.
3. To measure some constant parameters related to diffusion for experimental purposes, for example, measuring diffusion coefficient.

All micromixers fulfilling different motivations can be categorized into two types in the form of the type of energy source, which is passive and active. A passive micromixer relies entirely on pumping energy, whilst an active micromixer replies on pump energy and external energy input simultaneously, such as dielectrophoretic micromixer, electrokinetic micromixer, or acoustic micromixer [32].

One classic passive micromixer is a laminar micromixer, which principally consists of a long straight mixing channel and two supply channels. Depending on the degree of angle between two inlet microchannels, it is called ‘T-mixer,’ ‘Y-mixer,’ or even ‘Arrow-mixer’ (see Figure 7). The diffusion merely occurs in the middle mixing channel. As the factors determining the degree of diffusion have been discussed in Section 2.5.5, the length of the mixing path and the contact area are dominated factors in a passive micromixer. The original design of micromixer applying in this thesis is inspired by the laminar micromixer.

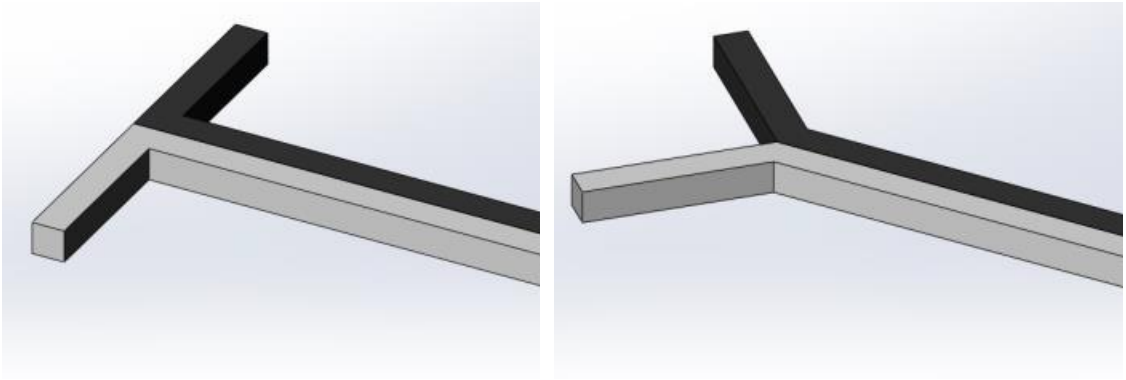

Figure 7. *'T-mixer' and 'Y-mixer' passive micromixers [28]*

In addition to pumping energy, an active micromixer also relies on one or more external energy inputs, varying in thermal energy, acoustic energy, electro-osmotic energy, and so on. For instance, Figure 8 shows a schematic diagram explaining how electro-osmotic active micromixer promotes mixing efficiency. Applying potentials on the electrodes fixed to the wall of a T-shaped micro-mixer, which directly changes flow profile in the channel and then increases mixing efficiency.

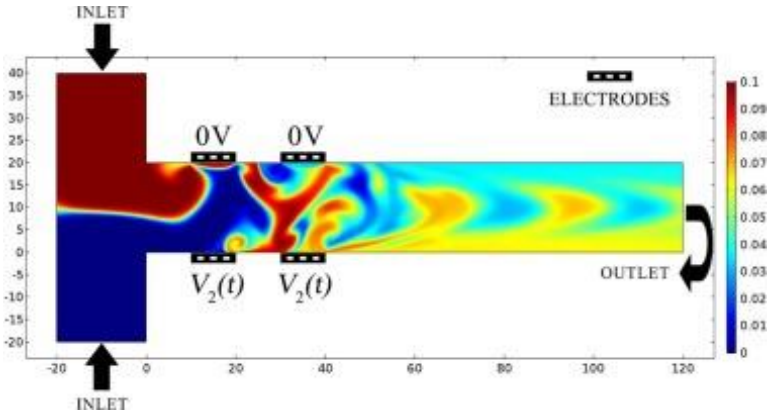

Figure 8. *Electro-osmotic active micromixer [33]*

Each type of micromixer is tailored to fit the intended application. The passive micromixer is more appropriate for approaching the non-mixing goal.

2.2.7 Shear stress

The continuous flow is essential to establish and maintain the required concentration gradient, so some properties of fluid accompanying flowing, like viscosity or shear stress, need to be highlighted. In the biomedical point of view, shear stress has been shown to increase the activity of osteoblasts on engineered scaffolds substantially [34] [35]. Mainly, shear stress deserves an emphatic consideration in this thesis as a cell's adhesion and shear stress need to be in a reasonable balance.

The viscosity is a direct result of shear force. When a shear force deforms a fluid, viscosity determines how fast the fluid deforms. The relationship between viscosity, shear stress, and shear rate is presented as:

$$\eta = \frac{F/A}{dv/dl}, \tag{17}$$

where *v* denotes fluid velocity, *l* means the position within the height of the microchannel, η means fluid viscosity, *F* refers to force, and *A* is cross-section area.

Viscosity is a fluid's capability resisting deformation, which is presented as a ratio of shear stress to shear rate. In the same way, shear stress can be calculated if viscosity and shear rate are given. Considering the height of microchannel is hundreds of micrometre, and cell's height is tens of micrometre, thus the ratio of cell height to microchannel height is less than 0.1. Thus, wall shear tress is approximately accounted as the shear stress applied to cells in some sense. It is given as:

$$\tau = \frac{h}{2}\left(\frac{\Delta P}{\Delta L}\right), \tag{18}$$

where τ denotes wall shear stress, h means the height of the channel, ΔL means the length of the channel, and ΔP refers to pressure drop.

Instead of approximately estimating shear stress by applying the formula of wall shear stress, in Chapter 3, a way of calculating shear stress by simulation will be demystified. Besides, comparing the values derived from approximate estimation and simulation has its profound validation as well.

2.3 Computational fluid dynamics

For some microfluidic applications in which the networks of channels are simple and straightforward, the Hagen–Poiseuille's law, a physical law that explains the hydraulic behaviour of pressure-driven flow through a circular channel are appropriate [36] [37]. However, as a network of microchannel becomes more and more complex, Hagen–Poiseuille's law gradually appears inadequacy when the irregular geometry and nonlinear property are involved. Thus, computational fluid dynamics (CFD) started to be applied to analyse the performance of the flow inside networks. Notably, it is used extensively as the rapid development of computer science. The CFD method is a simulation-based method that enables users to analyse numerical data of fluid in varying dimensional objects, like 1D, 2D, or 3D. The mathematical models for engineering or environmental objectives are established in CFD by a set of differential equations describing the relationship among physical quantities.

2.3.1 Discretization methods

Once the mathematical model has established, CFD will apply one discretization method to model, which enables the model to be calculated within small parts of geometrically simple shapes. The simplification of complicated questions is always one of the primary guiding principles. Typically, three main discretization methods embedded in most CFD software, which are Finite Volume Method (FVM), Finite Element Method (FEM), and

Finite Difference Method (FDM), respectively [38]. For instance, the ANSYS Fluent mainly uses FVM solver, which based on an integral form of the PDE to be solved, with the values of the conserved variables averaged across the volume [39]. COMSOL®, the simulation software, is based on FEM discretization dividing up the region into some of the finite elements for the computational domain [40]. Each method is quite similar in that it represents a systematic numerical method for solving partial differential equations (PDEs).

FEM is the default discretization method in the COMSOL Multiphysics®. It subdivides a Computer-Aided Design (CAD) model into very small but finite-sized elements of geometrically simple shapes. The collection of all these simple shapes constitutes the so-called finite-element mesh. Each element is defined by a set of points, which are referred to as nodes in the FEM (see Figure 9). [40] Each node can be mathematically represented by PDEs that describe the physics involved in the model. For example, in the case of fluid, PDEs are associated with the governing equations, NS equations. Adjacent nodes exist an action of transmitting information in sequence. The information includes shape function and primary physical function. Finally, when the contributions of all elements are assembled, an approximation of the real solution to the PDEs is generated.

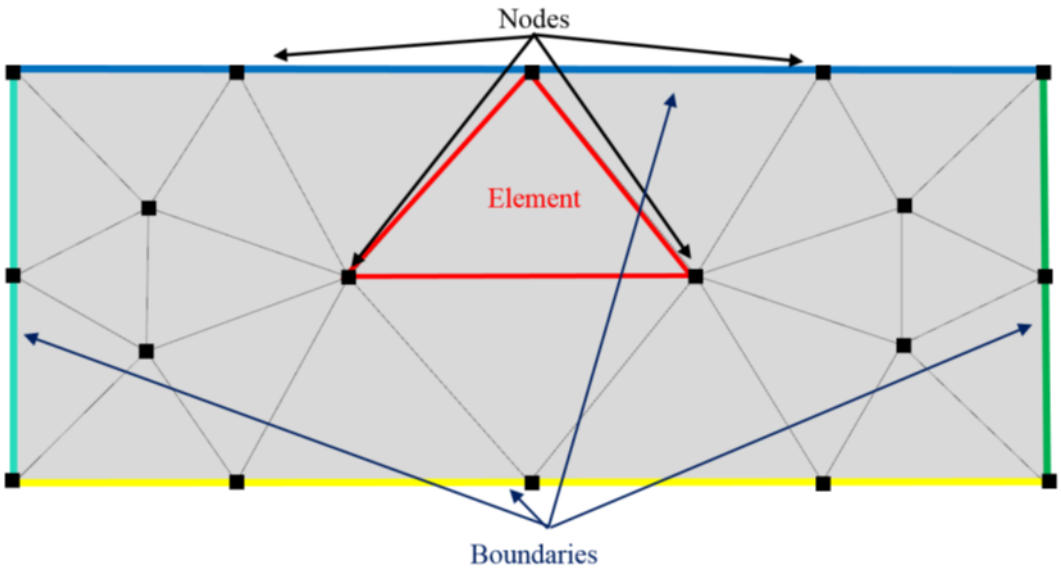

Figure 9. *A schematic of FEM [28]*

The reason that it is an approximation, not a real solution is most geometries PDEs cannot be solved with analytical methods. Instead, an approximation of the equations can be constructed based on different types of discretization. By way of illustration, when a domain to be solved is in a shape with some curved sides as below and the shape of a single element is quadrilateral, the shape function between two nodes cannot correctly match the curved sides in the first-order case. Precisely, the approximation derived from

the first-order element has a markable discretization error in comparison to the second-order case (see Figure 10). Typically, the higher- order of element applied, the more accurate approximation and the more massive computation load.

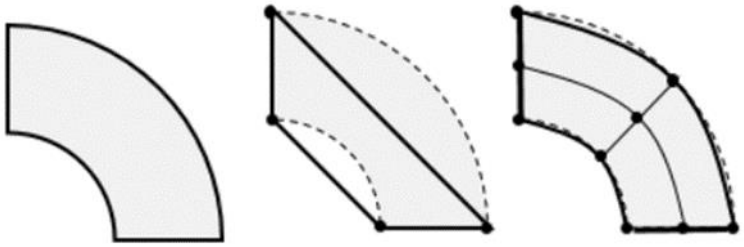

Figure 10. *A domain with curved sides. Single first- and second-order quadrilateral elements are applied [41]*

Instead of FEM subdividing models in small elements, FVM, just as its name implies, divides models into small volumes, which is well-known as cells. The FVM is based on conservation laws, which refers to what goes into one cell on one side needs to leave the same cell on another side. Following this idea, a formulation that consists of flux conservation equations will be defined in an averaged sense over the cells [42]. Different from FVM and FEM, FDM is typically defined on a regular grid which is not suitable for solving irregular CAD models, instead of for rectangular or block-shaped models.

Empirically, both FEM and FDM have been used very successful in solving the fluidic application. However, the FEM is comparatively suitable for multi-physics problems because it could combine different kinds of functions that approximate the solution within each element. This is the main reason that FEM has been selected to use in this thesis. Meanwhile, the FEM is usually most taxing on a computer system, but it depends on the type of analysis.

3. MATERIALS AND METHOD

In a microfluidics-based project, designing a reasonable channel network of a microfluidic chip is fundamental and essential to the subsequent stages. A good channel network must correlate with various biological or biomedical motivations over different applications. This thesis emphasizes a specific channel network that develop a distinctly 'straight' chemotactic gradient within a specific range of flow rates. The channel network is designed on account of mathematical considerations, which include *Re*, *Pe* and *Kn*, and some experimental constraints, such as shear stress, flow rate, mixing efficiency. Once the channel network was designed in the CAD and SolidWorks, the simulation model will be established in COMSOL Multiphysics® software based on CFD.

Since Whitesides' research group in the late 90s introduced a rapid prototyping method for fabricating microfluidic channels, this fabrication technique is widely used over the years, and without exception to this thesis. Precisely, this prototyping method can be divided into two phases, which are mold fabrication and PDMS replica molding. In the process of mold fabrication, a reusable mold is fabricated by patterning commercially available SU-8 resist onto glass or silicon wafer. Besides, the desired network of microfluidic channel is patterned on the wafer by applying photolithography. In the process of replica molding, the most commonly used PDMS in microfluidics, Sylgard 184 (Dow Corning, USA), is the preferred material fabricating microfluidic chips. Its attractive characteristics are biocompatibility, flexibility (elastic modulus ~ 2M Pa), optical transparency, to name but a few. When the PDMS-based microfluidic chip is in preparation, it will be treated with plasma and polyvinylpyrrolidone (PVP) to enhance its hydrophilization.

On the basis of a single chip, a conceptional platform for four parallel chips is presented further to facilitate the feasibility of contrast tests or parallel tests. Due to this platform has not been implemented, thus the fabrication process and assemble process will not be discussed in this thesis. The primary target is still a single chip's implementation.

The integrated microfluidic platform is set up after the sealed chemotactic chips are prepared. Briefly, the microfluidic platform in this thesis consists of a temperature control device for achieving constant temperature, a gas mixture cylinder for maintaining concentration of carbon dioxide, tubing for transferring liquid, hydraulic resistors for regulating flow rate, pump systems supplying power source, fluid sensor and pressure meter for measuring flow rate and pressure respectively. It is worth to mention that two pressure systems are applied during the experiments for different purposes, which are syringe

pump and pressure-based pump. The syringe pump system collaborates food colours solutes at the early stage of the project for experimentally testing and validating the feasibility of the integrated microfluidic platform. Then at the later stage of the project, pressure-based pump substitutes syringe pump, testing with the fluorescein isothiocyanate (FITC) under the microscope for validating the practical mixing gradient in comparison to simulation counterpart.

The comparative results between simulation and experiments surrounding the mixing efficiency are studied, after acquiring and processing the imaging data under the microscope. The experimental results are discussed in Chapter 4.

3.1 Microchannel design for mixing

For some applications that the requirement to mixing efficiency is close to fully-developed mixing, the laminar mixer does not appear a competitive advantage because it needs a sufficiently long mixing channel to reach the status of fully-developed mixing. Conversely, its simplicity and robustness are more appropriate to the applications whose requirements are close to non-mixing, which aligns with this thesis. The ideal non-mixing chemotactic gradient separates chemokine solution and buffers solution in the mixing channel, which benefits to straightforwardly judge cancer cells' chemotactic movement and then to judge the efficacy of drug candidates. Thus, the initial layout of the microchannel in this thesis is inspired by the laminar serial mixer.

3.1.1 Shape design

The symmetrical network of the channel is patterned on a 15 mm diameter circular chip. The shape design is built based on the five principles presented below (see Figure 11).

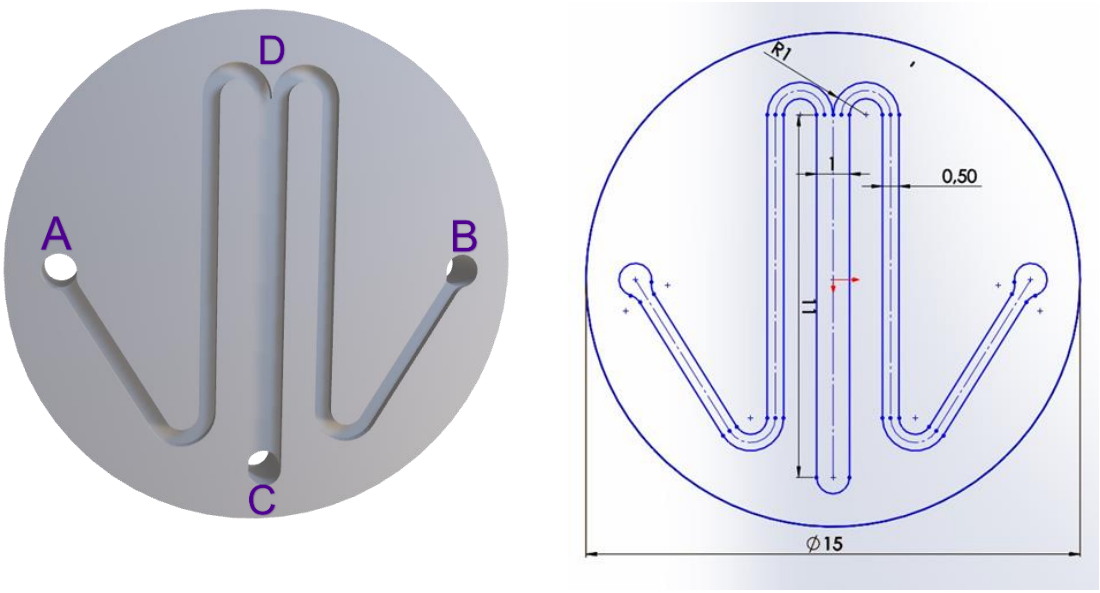

Figure 11. *A sketch of network of the channel*

1) An 11 mm mixing channel (C-D) placed in the middle of the substrate is mandatory for imaging chemotactic gradient and cell migrations. 2) Aim to achieve a high spatial utilization within a limited space, two inlets (A, B), one outlet (C) and the starting point of mixing channel (D) are designed in the four vertices (see Figure 6). Meanwhile, this distribution has a pragmatic purpose as well, which benefits the process of manually assembling tubing to microfluidic chips. If the inlets and outlet were placed next to each other, it is hard for a researcher to assemble the corresponding tubing quickly and carefully. In the course of experiments, two liquids are pumped into two inlets simultaneously, and then they will meet each other at the point (D). 3) As the target of this thesis is to form a chemotactic gradient as close to ideally non-mixing target or low mixing efficiency as possible, so to eliminate the mixing possibilities derived from convection is necessary. Thus, two semi-circle microchannels connecting the mixing channel are designed to enable the two liquids to flow as smooth as possible before mixing and then to flow as parallel as possible along the mixing channel after mixing. 4) Furthermore, two straight supply channels connecting two semi-circle parts are designed and placed in a parallel to the main channel. This distribution enables biologists to comparatively observe cell migration in three paralleled microchannels varying from different concentrations at the same time (see Figure 12). 5) In the end, the part of microchannel connecting to two inlets is designed on the basis of symmetrical aesthetics, and ideas from some typical applications, like Gradientech's cell culture chips, a microfluidic chip designed by Libing Dong's group [43] [44].

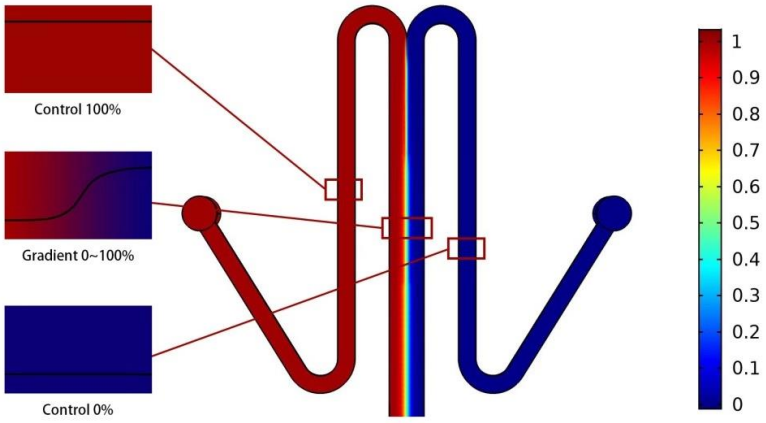

Figure 12. *Three parallel channels in different concentrations*

3.1.2 Dimension design

COMSOL Multiphysics®, one of powerful fluidic simulation software, computes the questions to dimension selection by applying lots of built-in formulas and some user-defined equations.

Initially, the height of the channel is 300 μm. The width of the mixing channel and two supply channels are 1mm and 500 μm, respectively. The initial dimensions selected by empirical instincts will be processed in an optimization study in the COMSOL® to implement a further optimal dimension. It is worth to mention that the dimension of microchannel not only depends on such factors as shear stress, flow rate, mixing efficiency, type of cell but also is determined by the volume of the reservoir, volume of a standard well plate if the conceptional four-chip-platform is considered. Thus, a comprehensive consideration between simulation results and practical operations is essential to decide the optimal dimension finally.

3.2 Simulation

Briefly, there are three principal simulation objectives in this thesis. The first one is to validate the hypothesis that the simulation results of the middle mixing channel about mixing efficiency approximately equals those results of the integrated geometry. If this hypothesis is valid, the computational load will be decreased dramatically. The simplification of complicated questions is always one of the primary guiding principles. The second one is to seek out the optimal dimensions of the microfluidic chip for the minimum mixing efficiency. Finally, the relationship among all significant parameters and variables are studied and summarized to support the practical experiments.

3.2.1 Simulation process

The simulation process in this thesis is merely implemented by the COMSOL Multiphysics®, which is a simulation platform that encompasses all of the steps in a consistent modelling workflow — from defining geometries, material properties, and the physics that describe specific phenomena to solving and postprocessing models for producing accurate and trustworthy results [40]. The users could rapidly master it, benefitting from its concise and open-and-shut operation interface. In the interface of the model builder, the modelling steps are presented step by step in a reasonable order. The modelling steps associated with this thesis is presented below in the order as in the model builder window.

1. Multiphysics selection

COMSOL Multiphysics®, as its name implies, is an analysing software for coupled multiple physics, which enables its users to select the interested physical modules, such modules as electrical, heat transfer, fluid flow, or even optimization. Notably, its compatibility with a self-construct physical module based on the PDEs module is very compelling. In other words, users could create their physical modules to satisfy various projects. In this thesis, the interface of laminar flow from the fluid flow module and the interface of transport of diluted species from chemical species transport are selected to solve several simulation objectives. Besides, the study is the stationary study, which is always used in the experiment in which the field variables do not change over time.

2. Model geometry construction and material selection

Geometry construction can be established by either directly importing a standard CAD file into COMSOL® through its 'Geometry' interface or modelling geometry by using built-in tools in the COMSOL®, which include solid object, surface, curve, and Boolean operation. Geometries are defined by sequences of operations, where each operation can receive input parameters for easy edits and parametric studies in Multiphysics models. Furthermore, material modelling. Compare to the model constructed by importing a CAD file, the model established step by step in the COMSOL® is more convenient to edit. The model simulated in this thesis is established in the COMSOL®. Then material modelling is setup, depending on the experiment emphasis. For instance, this experiment merely highlights the study related to fluid, regardless of the study of fluid-solid coupling. Thus, it is necessary to select water as a global material and then apply water in the integrated geometry, regardless of the material of microchannels. Figure 13 is a 3D modelling of the microfluidic chip constructed by COMSOL®.

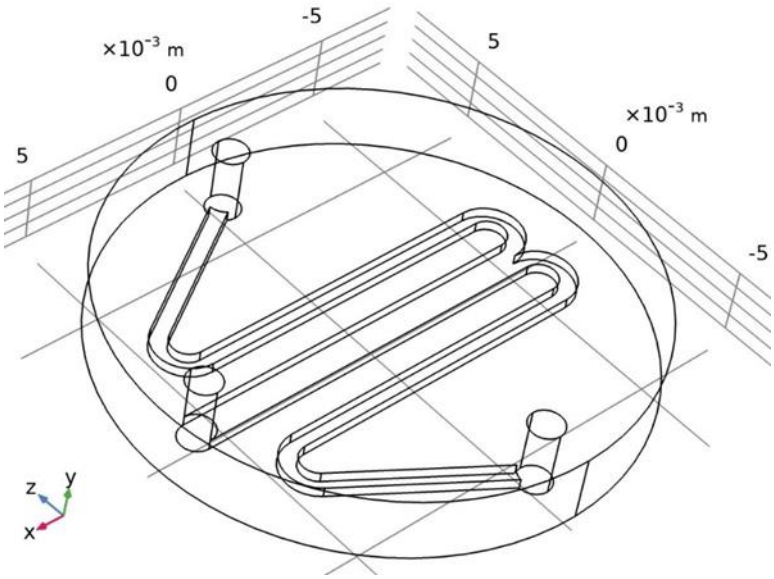

Figure 13. *Model geometry in the COMSOL®*

3. Settings for parameters, variables, initial condition, boundary condition

Although the selected Multiphysics modules offer systems of field equations, settings for specific requirements varying from applications are essential for a successful simulation system. The parameters and variables are defined under the branch of 'Global Definitions'. The parameters, in this case, are flow rate (initial 10 µl/min), dimensions of each part of the model, temperature (310.15 K), the diffusion coefficient of the FITC (80 $\mu m^2/s$), and concentration of FITC (1 mM). The variables are shear stress, mixing efficiency. The boundary conditions include 'no-slip', incompressible, continuous fluid, and all boundary conditions discussed in Section 2.2.3. The initial condition is referred to as the initial state of fluid and solutes in this case. Typically, the initial state of the fluid is considered as motionless until the pressure applies. The initial state of concentration is 0.

4. Meshing

The quality of meshing could affect directly to the accuracy of the solution. Once model geometry is constructed and described by partial differential equations, the solution to the mathematical model is approximated through the finite element method. According to the theoretical discussion on FEM in Section 2.3.1, the FEM is used to discretize the model into smaller, discrete parts. The solution is obtained through stitching together low order polynomials over each element to form a piecewise global function. In order to acquire the best approximation to the real solution, nothing is more significant than the way of meshing. COMSOL® provides various features and functionality to address meshing considerations. The user could choose either completely automates the process of meshing the geometry or building a custom mesh sequence by himself. Typically, a mesh

sequence consists of the mesh element type, size, and distribution of elements, element order, mesh quality.

The element type used is the shape, which is used to divide up geometry. By way of illustration in the different dimensional model, in the 1D model, the element shape is an interval. In the 2D model, the shape is either triangle or quadrilateral, with the default being a triangular element. For the 3D model, it can be tetrahedron, hexahedron, pyramid, or prism, with the default being a tetrahedral element. Outstandingly, the software makes several recommended default choices based on an empirical database, including the mesh element type used, depending on the physics that are involved in the model. For example, the model of this thesis is constructed by the physics, laminar flow, and transport of diluted species. Thus, the default element shape assigned by COMSOL® is triangular in 2D or pyramid in 3D.

Furthermore, the accuracy of the approximation is a direct result of the size and distribution of elements. Theoretically, a finer mesh will give more accurate results. However, this makes the problem more computationally demanding. The size of elements applied in the channel model depends on the degree of significance to study areas. Precisely, the meshes in the mixing channel where the diffusion happens are finer than those of in the supply channels. Besides, the mesh is finer along as it is approaching the mixing line, the line splits the mixing channel in half. This way of meshing shortens the simulation time exceedingly. Meanwhile, it is vital to use a suitable element discretization order for models as well. The discretization order used, which is done through the physics settings, affects the function which interpolates the solution between nodes. Mainly, for models included coupled physics, they need to take more considerations on the order of element discretization since different element order settings can be optimal when computing a Multiphysics problem. The flow discretization order to laminar flow is P2 + P1 in this model, which refers to the second-order interpolation for velocity, and the piecewise linear interpolation for pressure. The concentration discretization order to transport of diluted species is quartic interpolation for concentration.

When the user solves the model and the solver converges, this only means that got the best approximation that obtained with the meshing currently in use in the model. It does not tell that the solution is close enough to the solution of the mathematical model. Thus, to validate or verify the mesh element quality is necessary after initial meshing. Typically, either performing a manual mesh refinement study or asking COMSOL® to do it automatically through performing adaptive mesh refinement is achievable. Figure 14 shows the difference between physic-controlled mesh and user-controlled mesh visually.

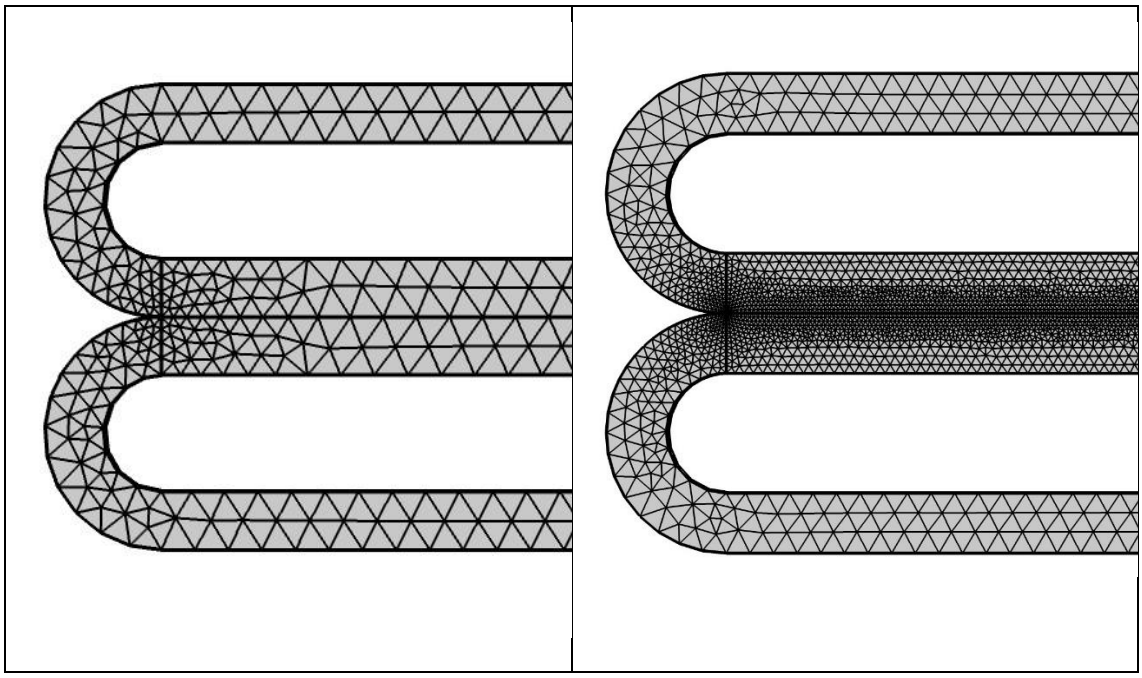

Figure 14. *Physic-controlled mesh VS User-controlled mesh*

5. Study and postprocess

COMSOL® provides two options to users in terms of the type of study, which are stationary and time-dependent. The stationary study refers to that only spatial partial derivatives are considered in the partial differential equations. Whereas, time-dependent study computes not only spatial partial derivatives but also the partial derivatives in time. The flow applied in this microfluidic system is at least a 24-hour-long continuous flow. Thus, the stationary study is suitable. As the discretization method discussed in Section 2.3.1, FEM ends up with a discrete equation matrix of linear algebra. Then, by employing a solver to solve equation matrix and finally acquire an approximation to the real solution. When it comes to the solvers, there are two types of solvers available, which are direct solver and iterative solver. The direct solvers can be used for small- and midrange-sized problems, while the iterative solvers can be used for larger linear systems. Typical, the default solver in the laminar flow interface is Parallel Direct Sparse Solver Interface (PARDISO), a direct solver. This solver is competent in the simulation for this thesis. Sometimes, in order to improve the accuracy of the approximation, the solver setting is changed and configured manually under each solver node to tune the performance for solving a specific problem.

Two functions (optimization module and parametric sweep) under the ‘Study’ interface are employed in this thesis to solve two simulation objectives, which are optimal dimension and mathematical relationship among flow rate, mixing efficiency, and shear stress. The optimization module is an optimization tool benefiting to analysing optimal dimension or shape to models. Typically, it involves four steps to solve optimization problems. First,

to define the objective function is a prerequisite. The objective function of this model is the mixing efficiency function, which is mathematically defined in Section 2.2.5.

$$S = 1 - \frac{\left(\int_{A_x} |C_x - C_\infty| \, dA_x\right)/A_x}{\left(\int_{A_i} |C_i - C_\infty| \, dA_i\right)/A_i} \tag{15}$$

Second, a set of dimensional variables are specified, which include the height of microchannel (100 μm – 500 μm), the width of the middle mixing channel (500 μm – 1 mm). Third, to set up a set of constraints to bound on design variables. The primary constraint in this model is the magnitude of shear stress, which must be less than 0.01 Pa, which indirectly determines the selection to flow rate [45]. In addition to having a risk of flushing tested cancer cells away, some articles have been shown that high shear stress influences cancer cell's adhesion and chemotaxis induction [46] [47] [48]. In order to minimise the effect of shear stress on experimental data, the limitation of shear stress is less than 0.01 Pa. The shear stress can be expressed as shear rate (spf.sr) times fluid viscosity (spf.mu) in the COMSOL®. In the end, using optimization function improves the design based on constraints.

The other function is parametric sweep, which is applied to study the mathematical relationship between two parameters - flow rate (1-20 μl/min), the height of channel (50-300 μm), and two variables - mixing efficiency, and shear stress. The interval between each flow rate is 1 μl/min. The interval between each height selection is 50 μm. All combinations between flow rate and height of the channel are executed one by one once the setup is ready.

The postprocessing interface has versatile functions enabling users to present results in different manners, ranging in table, 3D figure, 2D figure, and 1D figure. The results in detail are presented and demystified in Chapter 4.

3.3 Microfabrication method

The microfabrication method employed in this thesis is a soft lithography-based method to prepare microfluidic chips from PDMS, which has been extensively used in various microfluidic applications. Empirically, a mature soft lithography-based method consists of the following processes in sequence, starting from replica mold fabrication, through chips replica molding and ending to plasma treatment, and hydrophilization treatment, depending on the requirement of experiment. Its advantages include high flexibility in the course of fabrication, low cost, high-resolution geometry. In general, new mold can be implemented within 24 hours. Although the emphasis of this thesis is not microfabrication

method, the microfabrication method is theorized summarily (see Figure 15) in consideration of coherence and consistency of thesis.

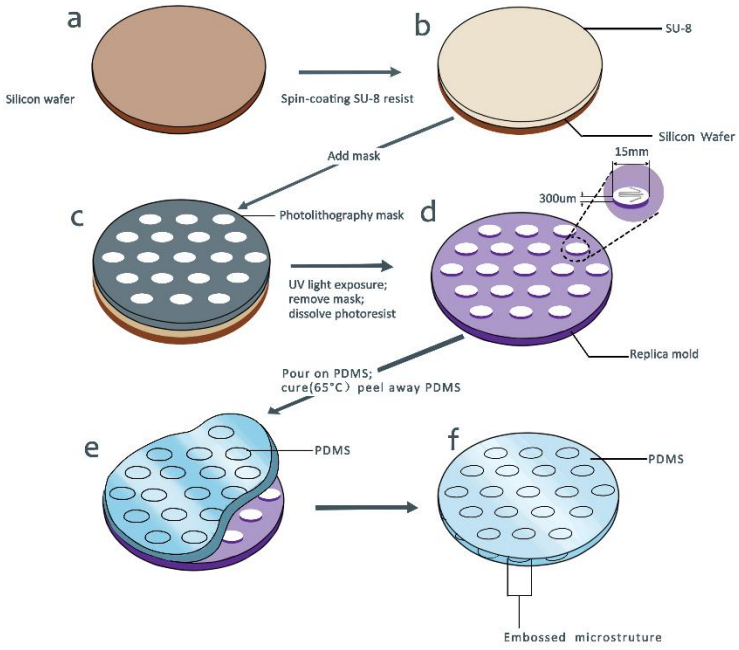

Figure 15. *Fabrication of a PDMS layer incorporating microchannels. Drawings (a) – (d) correspond to the fabrication of a SU-8 mold via photolithography. Drawings (e) and (f) can be considered as part of the soft lithography process*

3.3.1 Replica mold fabrication

The soft lithography-based method is widely employed to fabricate the replica mold when the structural dimension of mold at the microscale [2]. Whereas, for the smaller dimension, electron beam lithography is more suitable, although it appears to be time-consuming and high cost. Considering the biomedical motivations of this thesis, which is to study cell migration, so the minimum structural dimension of the microchannel should be more than 100 μm. Thus, the soft lithography- based method is in priority.

Shortly, there are four steps for fabricating a replica mold by a rapid prototype, which are: i) designing and printing of a photolithography mask, ii) spin coating of SU-8, iii) photolithography, and iv) development of the resist structure. The CAD file of the microchannel firstly imports to the μPG 501, a delicate micro pattern generator for low volume mask making [49]. After the file conversion is finished by setting through μPG 501's user interface, a blank mask will be exposed for printing pattern on and will turn to be a patterned photolithography mask. Then, selecting a silicon wafer as base substrate and spin-coating by pouring the SU-8, an epoxy-based negative photoresist that is widely applied in the fabrication of microstructure, on the wafer substrate.

SU-8 shows excellent biocompatibility and chemical stability. Mainly, its Young's modulus is 5 GPa, and the temperature to thermal decomposition is 380℃, which is suitable to be a material for the microstructure in a high resolution, as well as a high aspect ratio (15:1) [49] [50]. The thickness of the SU-8 layer on the wafer substrate highly depends on the spinning speed used.

In the photolithography step, J500 VIS (OAI, USA), a mask aligner device is used to expose the wafer coated by SU-8 to ultraviolet (UV) light. The patterned photolithography mask is placed between the UV light source and the wafer substrate. The purpose of the mask is to confine the UV exposure merely applying in the specific areas of the resist layer. In the end, the photoresist structure on a base wafer is developed by immersing it into the mr-DEV 600 developer solution to convert the latent image to a visible image.

Figure 16. *SU-8 mold in the process of photolithography*

Of note, the microfabrication method based on SU-8 lithography can merely fabricate the structures with a vertical sidewall.

3.3.2 Chips replica molding

Sylgard 184 (Dow Corning, USA) is the type of PDMS used in this microfluidic chip. Its characteristics are flexibility (elastic modulus is 2 MPa), low surface free energy (2.16E-2 J/m^2), biocompatibility, and optical transparency down to 280 nm [51]. The high flexibility enables PDMS structure to be manipulated effortlessly in comparison to glass. Its low surface free energy reflects in the chemical inertness that the PDMS chip can be repeatedly used by a few months. The plasma-treated PDMS exhibits hydrophilicity temporarily, instead of its original surface property, hydrophobicity [52].

Before casting PDMS onto the SU-8 mold, the base part of PDMS is sufficiently mixed with its curing agent in the ratio of 10:1. Since considerable air gets trapped in the PDMS material during the mixing process, thus degassing is necessary. The degassing process is implemented by placing the SU-8 mold with PDMS into a vacuum chamber. And then curing the degassed PDMS in the oven over 10 hours, 65℃. It is worth to highlight that the pattern on the PDMS layer is a mirror pattern on the SU-8 mold. Thus, in the process of designing geometry on the AutoCAD, it is necessary to take consideration.

3.3.3 Plasma treatment

As Figure 16 shown, the pattern of the SU-8 mold consists of a few identical chips' patterns. For the purpose of acquiring an elaborate PDMS chip, the entire PDMS layer is firstly peeled off from SU-8 mold along the edge, and then the PDMS chip is punched out from the PDMS layer by using a 1.5 cm hole punch. Whereas, a fancy microfluidic chip consists of a PDMS chip, as well as a glass substrate. Before to treat the PDMS chip by the oxygen plasma for bonding with a glass substrate, it is necessary to punch two inlets and one outlet on each chip by using a 0.8 mm hole punch. Then cleaning the PDMS surface with isopropanol and scotch tape to make sure there is no dust, oil, or dirt residue remaining on the surface of each chip. A sanitary and dried chip is the prerequisite of plasma treatment.

Owing to pristine PDMS characterizes low surface energy, in this thesis, an oxygen plasma treatment is arranged to activate its potential surface energy by the Diener PICO plasma cleaner [53]. In the process of oxygen plasma boding, the silanol groups (-OH) at the surface of the PDMS layers are exposed gradually that they form strong covalent bonds (Si–O–Si) when brought together with glass (see Figure 17). These covalent bonds form the basis of a practically inseparable seal between the layers [54]. Theoretically, the bonding status would remain effective over a long period.

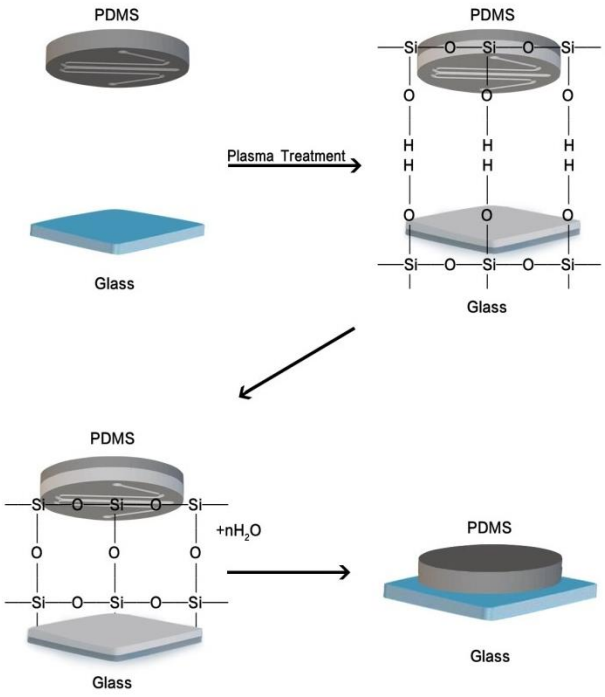

Figure 17. *A schematic diagram of plasma bonding*

3.3.4 Hydrophilization of chips

As discussed before, untreated PDMS material is hydrophobic, which may cause inconvenience during the experiments. Mainly, applying in the case of a microfluidic system, the disadvantages of hydrophobic PDMS are the rather extensive bubbles trapping and poor cell adhesion [55] [56]. For improving the wetting properties of PDMS, many published studies present that using radiofrequency (RF) oxygen plasma could activate the PDMS surface. Pasi Kallio's group has validated that only treating oxygen plasma with PDMS could not maintain its hydrophilicity in a long term because of the effect of hydrophobic recovery. As data reveal, the wetting of PDMS up to 5000 min of aging, which is not suitable for a long experimental cycle. Thus, one more hydrophilization treatment is added in this thesis, a way of coating polyvinylpyrrolidone (PVP) solution on plasma-treated chips, which is referenced from article published by Pasi Kallio's group. According to the results, the PDMS surface persists hydrophilicity at least six months. [57]

For the PVP solution used in the experiments, a 22.2% (w/v) solution of polyvidone 25 (Merck MGaA, Germany) was prepared in DI-water. Once the chips are taken out from the plasma cleaner, the PVP solution is recommended to syringe into the microchannel from one of the inlets immediately. Because the effect of hydrophobic recovery increases gradually as time goes by. According to the dimension of the microchannel, 10 µl PVP

solution is enough for this PDMS chip. Then, vacuum out the PVP solution and clean the residual PVP solution in the microchannels by DI-water in ten minutes.

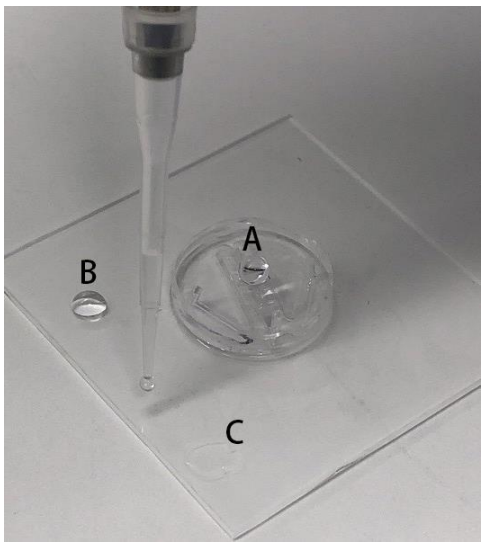

Figure 18. *Hydrophobicity (A and B) and hydrophilicity (C) on a chip*

Figure 18 shows that the areas of the glass substrate and PDMS chip activated by oxygen plasma displayed hydrophilic characteristics (C). Whereas, the areas not exposed to oxygen plasma remain hydrophobic characteristics (A and B).

3.4 Conceptional platform for four parallel chips

For some experiments that a single sample can fulfil the objectives, it is not necessary to test more samples in a parallel. However, for a versatile microfluidic platform that aims to cover every possible experimental objective, the specific setup to test several chips simultaneously is essential. Thus, to achieve a high throughput experiment that four chips can be monitored and imaged simultaneously under a microscope, a rational and logical layout should be designed in the standard size of a well plate footprint. The standard dimension of the footprint has established by the Society for Laboratory Automation and Screening (SLAS) (see Figure 19).

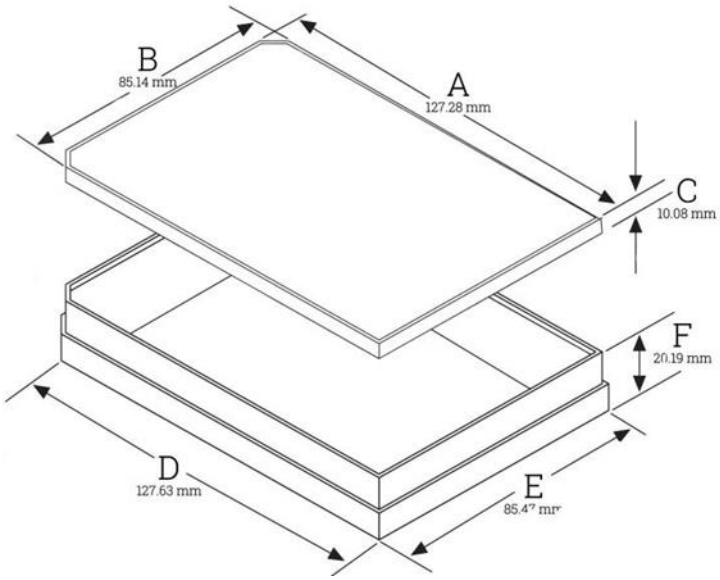

Figure 19. *The standard dimension of well plate footprint*

A, B, C are the length, width, the height of lid, respectively. D, E, F refer to length, width, as well as the height of the plate.

The core variable impacting the layout is the magnitude of the flow rate applied in the experiment. Besides, according to the fixed size of chip and footprint, and a series of experimental requirements, the ideally maximum flow rate applied in the footprint can be calculated. Precisely, assume the chips are bonded to a squared glass substrate (20 mm*20 mm). Thus, all four chips occupy 1600 mm^2 out of the approximate total floor area of the footprint, 10837 mm^2. The rest of the vacant floor area is 9237 mm^2, and then the available volume of the footprint is 186495 mm^3 if nothing blocks the chips. Furthermore, assume the experiment will last 24 hours and four identical size of reservoirs are responsible for storing two solutions to be pumped into chips and for accommodating waste solutions, respectively. Thus, the ideally maximum flow rate in one minute can be calculated as below.

Ideally, maximum flow rate = (186495 mm^3 ÷24 h÷60 mins÷4 reservoirs÷4 chips)× 2 inlets = approximate 16 µl/min. However, the ideally maximum flow rate is a direct result of a 100% space utilization. Practically, 50% - 60% of space utilization is promising over different constraints, such as the shape of reservoir, the tubing arrangement, the fixed structure, the thickness of the lid of a reservoir. By way of illustration, Figure 20 shows a theoretical layout which have not implemented in the practical experiment yet. The shape of the reservoirs is cylindrical, and four chips are placed in the shape of a square.

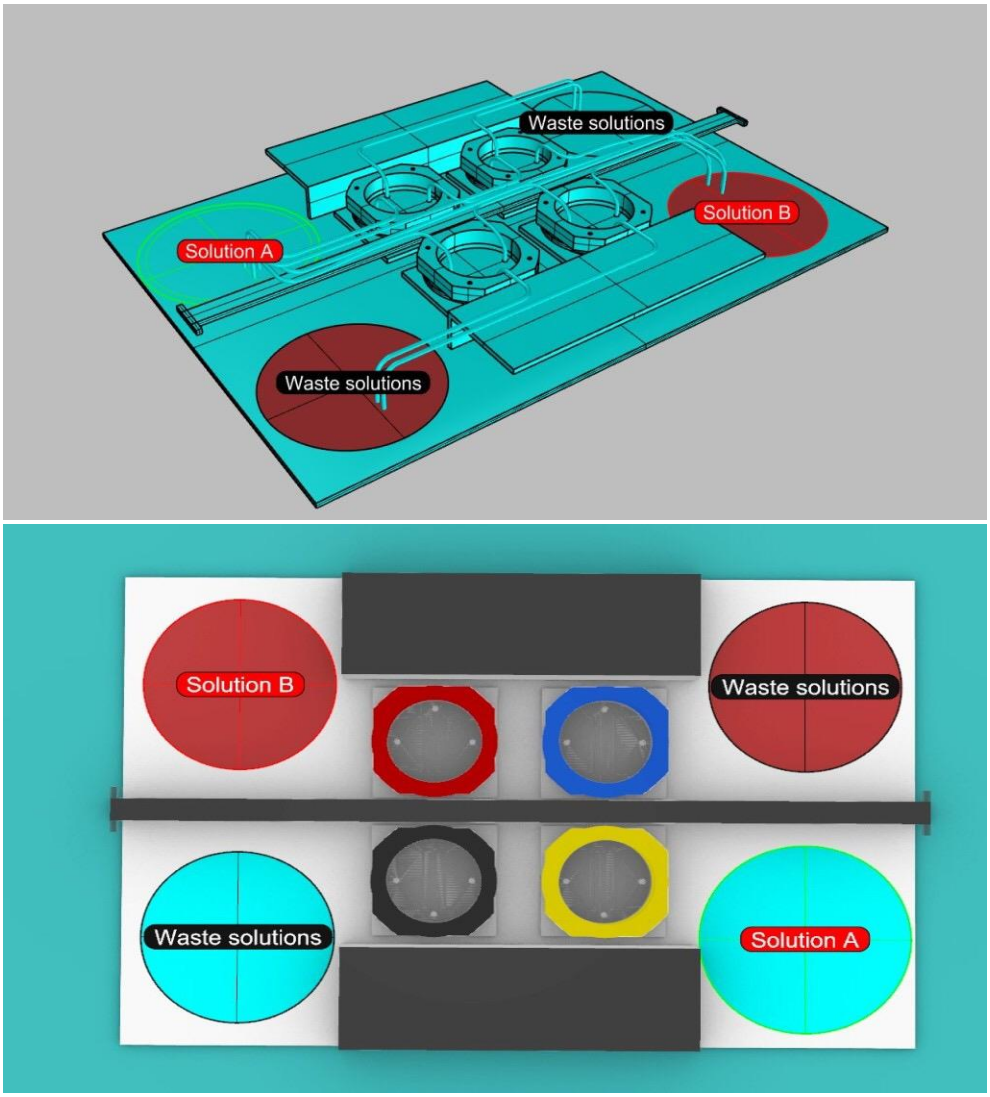

Figure 20. *The conceptional layout of chips and tubing in a well plate footprint*

3.5 Integration of the microfluidic platform

The microfluidic platforms aspiring to execute cell migration studies under the specific range of flow rate consists of five main parts, which are pump system, control system, accessories, and microscope. Depending on different experimental objectives, two microfluidic platforms are set up.

The first platform based on the syringe pump is studied for preliminarily testing the manipulative and experimental feasibility (See Figure 21). The solutes used in the experiments are two heterochromatic food colours. Although the experimental data or images derived from this microfluidic platform is not consistent with counterparts from simulation, it demonstrates that the theory of this microfluidic project is feasible and practical. Besides, the syringe pump system is of ease of the implements comparatively.

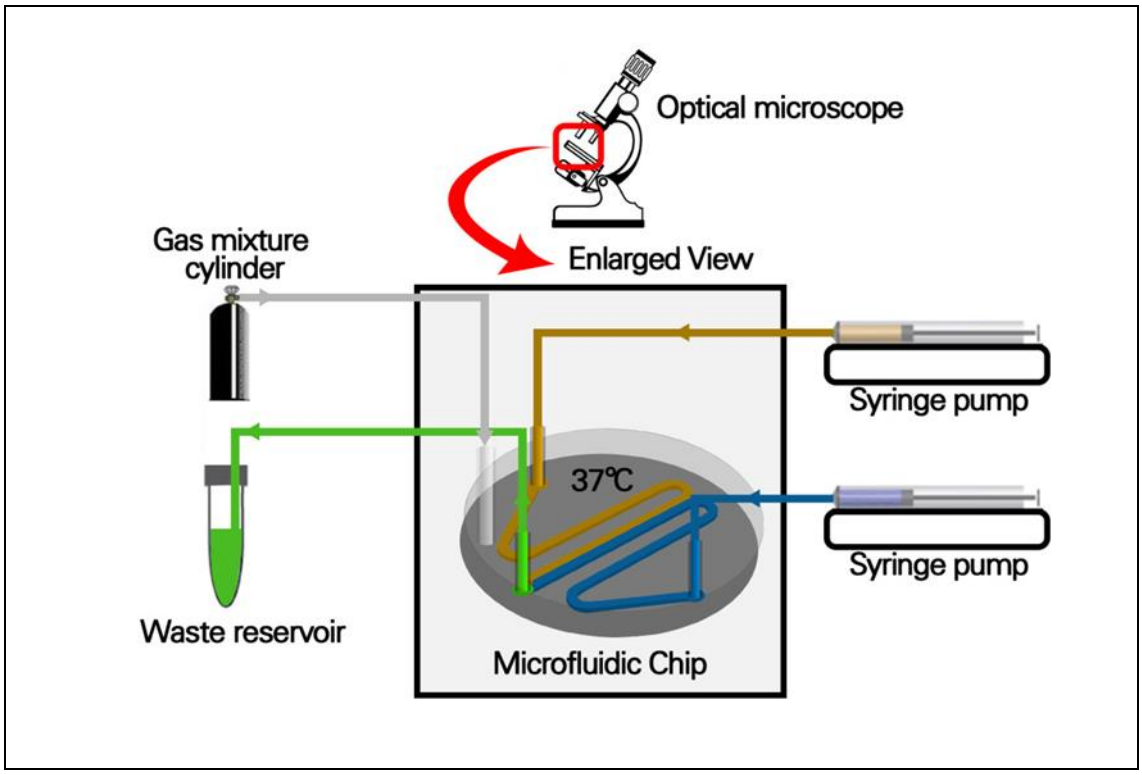

Figure 21. *The schematic diagram of the syringe-based platform*

The other platform based on the pressure-based pump is established since the success of the syringe one. In addition to changing the pump system from syringe-based to pressure-based, there is series of changes in terms of accessories, adding accessories like reservoirs, hydraulic resistors, flow sensors (see Figure 22 and Figure 23).

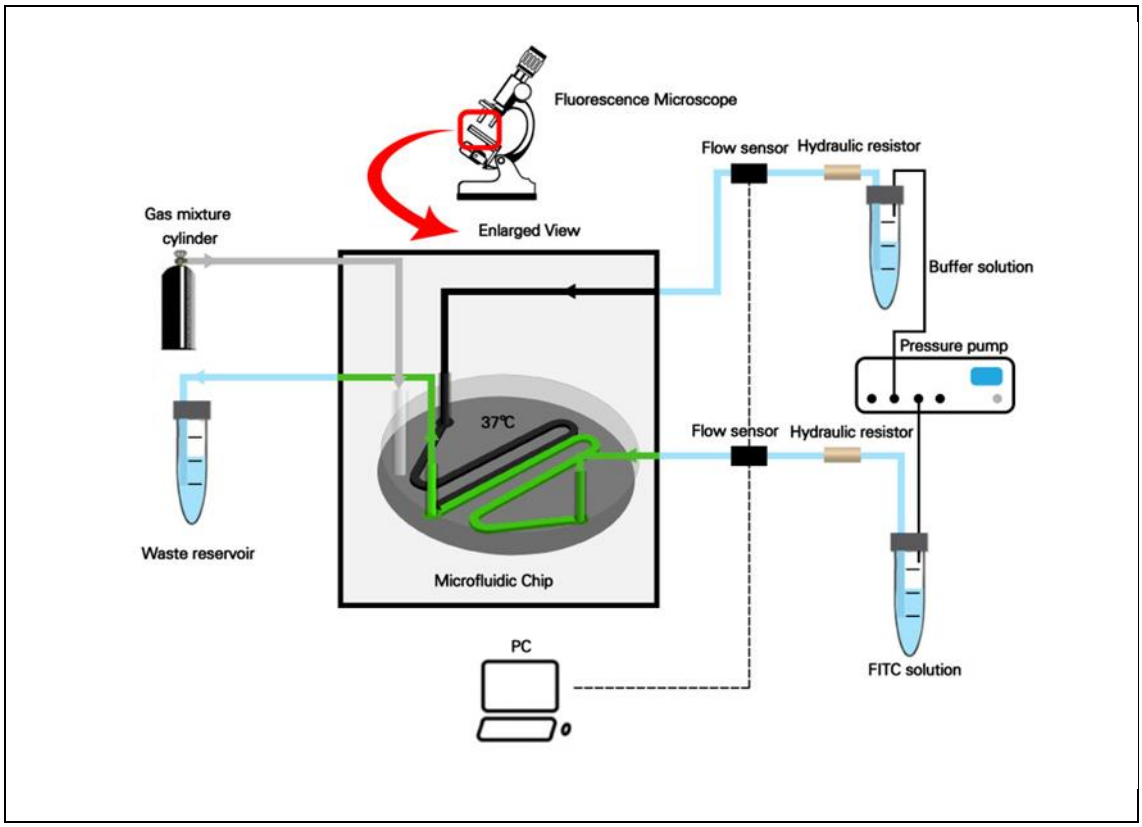

Figure 22. *The schematic diagram of the pressure-based platform*

Figure 23. *Critical components of two microfluidic platforms*

3.5.1 Pump system

The pump systems widely employed in the microfluidics studies can be categorized based on driving mechanisms into two types, passive pumps or active pumps. Although

the passive pumps, like gravity-driven flow or surface tension-driven flow, show outstanding competitiveness on the ease of implementation, accurate flow control is a priority among priorities in this thesis. Thus, the active pumps, syringe pump and pressure-based pump are employed to deliver a steady and relatively unchanging laminar flow rate to microfluidic chips once the value of flow rate has been specified in the user interface of a syringe pump or the meter of a pressure pump. Whereas, rendering active pumps needs relative complexity in initial setup and operational requirements before launching [58].

In the preliminary experiments, the NE-4501 syringe pump (New Era Pump Systems, USA), a purpose double syringe pump capable of infusion and withdrawal, is assigned to execute flow control (See Figure 23(1#)). It is controlled from a microcontroller-based system which drives a step motor, allowing an extensive range of pumping rates configured to the inside diameter of the loaded syringe. Considering the range of flow rate going to be perfused in the microfluidic chip and the diameter table in the user manual of the syringe pump, the volume of the loaded syringe selected for this experiment is 1 mL for each. The solutes are food colours from Dr.Oetker, a food supplier in Finland. The dilution is 1:5 between solute and DI-water.

The syringe pump is capable of accurately controlling the flow rate to change in a unit of 0.1 μl/min. And the simplicity in terms of assembling microfluidic platform is more compelling in comparison to pressure-based pump. The pressure-based pump controls the flow rate by cooperating with hydraulic resistors. A flow sensor must be assigned at the end of the tubing to validate the accuracy of flow velocity.

Comparatively, the syringe pump is more suitable for the preliminary tests. However, a critical limitation of syringe pump is the volume of a solution enclosed within a syringe is not infinite. For a long-term experiment, it is hard to achieve to disassemble syringes from the pump while maintaining the liquid flowing. Furthermore, the bubbles generated in the process of manually filling in the syringes could not be avoided or eliminated effectively by far. The massive residual bubbles in the syringes influence the cell's migration dramatically or even flush the adhered cancer cells away. Thus, the pressure-based pump is employed in the second stage to substitute the syringe pump.

The pressure-based pump, as its name implies that a pump that moves the fluid by gas pressure. The pump gauge associated with a pressure knob could achieve to roughly control the pressure in a range of 0 to 1 bar. Furthermore, one of the pump gauge's interfaces connects with a reservoir filled with gradient maker FITC, and a reservoir filled with DI-water through the tubing. It is worth to mention that the FITC solution is a 1:50

dilution and its reservoir is covered by aluminium foil to avoid emission happening under the bright light in the experiments. Then, as the pressure appears in the pump gauges, the solutions will be pumped and flow into chips finally.

3.5.2 Control system

In general, the control system in this thesis includes two ways of regulating the flow rate. Continue the discussion related to syringe pump in Section 3.5.1, the way of controlling flow rate is by remotely specifying parameters on the *WinPump Term* software. The regularly operational functions of a syringe pump, such as rate function, fill function, withdraw function has been pre-defined in the pump that users could regulate commands effortlessly and accurately. Whereas the way of controlling the flow rate by the pressure-based pump is relatively complex, which needs a series of accessories cooperating. There are two main accessories indispensable, which are hydraulic resistors for controlling the values of flow rate, as well as a flow sensor for measuring and validating flow errors between the practical velocity of flow and calculated values.

The mathematical relationship that a hydraulic resistance impacting on the velocity of flow can be clarified by applying the Hagen–Poiseuille's law. This law is a hydraulic–electric circuit analogy derived from Ohm's law in the electric circuit. In analogy with Ohm's law that voltage drop equals current times electric resistance, the equation of fluid dynamics that the pressure drop equals flow rate times hydraulic resistance is appropriate for the condition concerning the flow is laminar, Newtonian, and incompressible.

The hydraulic resistance is subjected to hydraulic resistor's characteristic dimensions, like radius in a circular cross-sectional channel, or length of channel, and the viscosity of fluid flowing through it. Depends on the different shapes of cross-sectional channel, it has different mathematical expressions. As a result of all hydraulic resistors (IDEX Health & Science, USA) and tubing connecting microfluidic chips applied in the experiments are of circular cross-sections, thus merely the expression which is appropriate to circular condition is discussed.

$$\Delta P = Q \cdot \frac{8\eta L}{\pi a^4}, \tag{18}$$

where the variable *a* is a radius of circular channel, *L* refers to the length of channel, ΔP refers to pressure drop, and η refers to viscosity.

By way of illustration, if the targeted flow rate, supply pressure, and the radius of hydraulic resistor are given, the user can regulate hydraulic resistor to keep both flow rate and pressure in a balance by adjusting the length of channel. There is no doubt that the practical value of hydraulic resistance is not identical to the calculated value. The reason

is not only because of the length error generating from manually cutting, but also tubing has a possibility of getting blocked in varying degrees during the manipulation. Thus, a flow sensor (Sensirion, Switzerland) is assembled to measure the practical flow rate at the end of tubing before the liquid flows into the channel. Due to the accuracy of the flow rate in consideration is in the unit of 0.5 µl/min. Thus, the tolerance in $\pm$ 0.5 µl/min can be accepted.

3.5.3 Gas supply & Temperature control

By volume, dry air contains only 0.04% carbon dioxide, which does not meet the experimental requirement, 5%. A certain amount of carbon dioxide could restraint the acid-oriented tendency, as most types of cell favour a slightly alkaline environment [59]. A gas mixture cylinder is employed to regulate the content of carbon dioxide all the time during experiments (See Figure 23 (13#)). The composition of the gas mixture is 5% carbon dioxide, 19% oxygen, and nitrogen. The gas supply tubing is placed above the microfluidic chip, maintaining the content of carbon dioxide based on the excellent gas permeability of PDMS (see Figure 21 and Figure 22) [60].

The heating device that regulates the temperature in the process of experiments includes a heat plate, H601-K-FRAME-GLASS-FLAT (OKOLAB, USA), and its corresponding heating controller. The heating plate employs Indium Tin Oxide (ITO) coating to obtain uniform heating throughout the glass surface. The controller with a touch screen interface enables users to control independently and accurately up to two heating devices (see Figure 23 (14# and 15#)). Temperature sensor and self-calibration routines allow easy calibration of the heating devices for the highest accuracy on sample temperature. During the experiments, the temperature applied on the chip is 37℃, which is maintained in the full process.[61]

3.5.4 Main accessories

Tubing as bridge connecting devices is a foundation for the microfluidic platform. The tubing used in the experiments is either made of PVC or silicone, depending on the experimental requirements. Besides, the inner diameter is typically 1 mm. In the pressure-based platform, the pressure presses the gas to the reservoirs through the tubing. Meantime, the solutions in the reservoirs are pumped out and start to flow towards the T-connectors. Once the flow reaches the T-connectors, the flow will be divided into four identical sub-flows in terms of flow rate. Then, the flows go through the hydraulic resistors, inlet connectors, and finally flow into the microfluidic chips, which are under the microscope.

3.5.5 Microscope setup

Before observing the chip under the microscope, the chip needs to be fixed in a holder plate, which will be assembled to the inverted microscope, AxioObserver Z1 (ZEISS, Germany). Different from ordinary bright-field imaging, the experiments involved with FITC requires a mercury short arc lamp to activate the emission of fluorescence at 518 nm wavelength.[62] FITC as the most common fluorescent reagents for biological research benefits by its high absorptivity, excellent fluorescence quantum yield, and good water solubility [63].

The magnification is set in 5x based on the dimension of images. The image of the integrated geometry of the chip is divided into some identical size of tiles under the microscope. The number of tiles firmly depends on the degree of magnification and the dimension of the chip. The microscope processes the image tile by tile. Typically, the more tiles, the longer the processing time. In the end, the integrated image consisting of several tiles is built.

4. RESULT AND DISCUSSION

The cumulative results from simulation and experiments are comparatively presented and illustrated progressively in order as below.

1. The simulation-based comparison between the integrated geometry and the straight mixing channel indicates whether the values of mixing efficiency in the straight mixing channel approximate those of in the integrated geometry or not. If the difference in mixing efficiency is within a range of 0.5%, the results of the straight channel approximately equal the results of the integrated channel. The efficiency of computation in the COMSOL® software will be improved dramatically. If not, repeat the process of comparison until the geometry which meet the 0.5% tolerance to the straight channel is determined. This process is the prerequisite for the following simulations, such as dimension optimization. The types of dimension will be explicit after the geometry is determined.
2. The optimal dimension of the chip is comprehensively analysed based on the results derived from the 'dimension optimization' function, and the consideration of the conceptional platform for four parallel chips.
3. The mathematical relationships between flow rate and mixing efficiency in a limit magnitude of shear stress are discussed based on the results from the function 'parametric sweep'. All these data from the simulation are the foundation of a successfully validated experiment.
4. Comparing the simulation results and experimental results gathered to validate the accuracy and precision of simulation is the last part of this thesis.

In the end, the merits and defects of two microfluidic platforms, and the improvements are discussed.

4.1 Geometry selection

On account of the laminar mixer, which only consists of a straight channel with two supply channels, this structure is fit to use in the experiment that pursuing the non- mixing status. The influence factors to diffusion efficiency have been appropriately illustrated in Section 2.2.5. Then, it is not hard to come out with a hypothesis that the dimensions of the straight channel dominate the degree of mixing, while the rest parts of geometry's influence marginally to mixing efficiency. Thus, two simulations, the straight channel and the integrated geometry, regarding the comparison in mixing efficiency are computed to validate the

hypothesis. If the hypothesis is tenable, it will reduce the computation load of simulations in the future. Simplifying is the best equation to solve the problem of issue complexity. Then, the focus of the study is more of the straight channel in the following simulations. If the hypothesis does not stand, the comparisons regarding the mixing efficiency between the straight channel and for example, 90% or 80% of the integrated geometry will be executed iteratively until the most dominated parts of geometry to the mixing efficiency is found.

The parameters applied in the two simulations and meshes constructed in the straight mixing channel are approximately identical. The dimensional parameters are 300 μm global height, 500 μm supply channels' width, as well we 1 mm straight channel's width. Besides, the default parameters applied in all simulations are 310.15 K temperature, 80 $\mu m^2/s$ diffusion coefficient of the FITC, and 1 mM concentration of FITC. Figure 24 illustrates the distribution of concentrations (right) and flow profiles (left) in the confluent cross-section and the outlet cross-section of the integrated geometry. Figure 25 illustrates those in the straight channel.

Visually, not only the shape of the concentration gradient or flow profile but also the magnitude is nearly the same in the two simulations. The shape of flow profile in the confluent cross-section, ranging in 10 to 20 μl/min flow rate, approximately consists of two identical parabolas, which refers to two separated Poiseuille flows. As the flow rate increases, the velocity magnitude of Poiseuille flows will increase. In the outlet cross-section, the shape of the flow profile characterizes one gentle parabola, instead of two. The two separated Poiseuille flows gradually integrate into one flow along the channel. Comparatively, the shape of flow profiles in the confluent cross-section has a slight difference between the two simulations. In the integrated geometry, the peak of flow profiles trends to be slight two sides skew resulting from the centrifugal forces generated when the fluid flow through the curving channels. In contrast, those in the straight channel do not have this trend. However, this slight difference in the flow profile does not affect too much to the mixing efficiency.

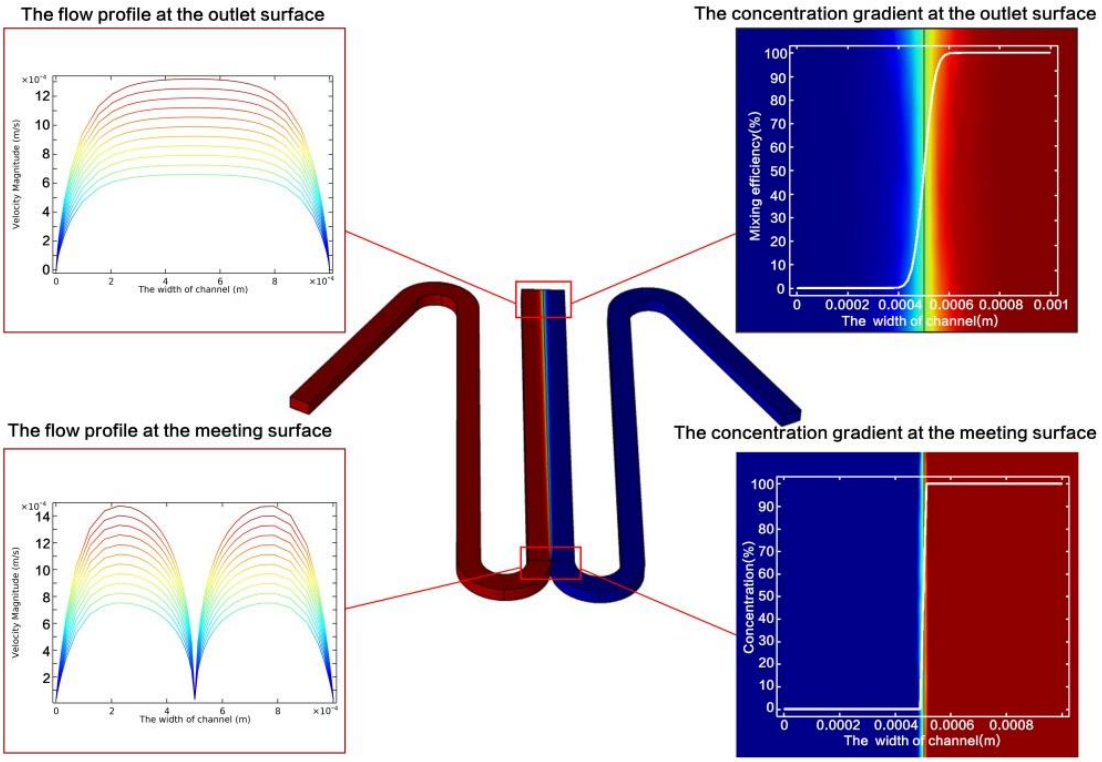

Figure 24. *The characteristics of flow and diffusion in the integrated geometry*

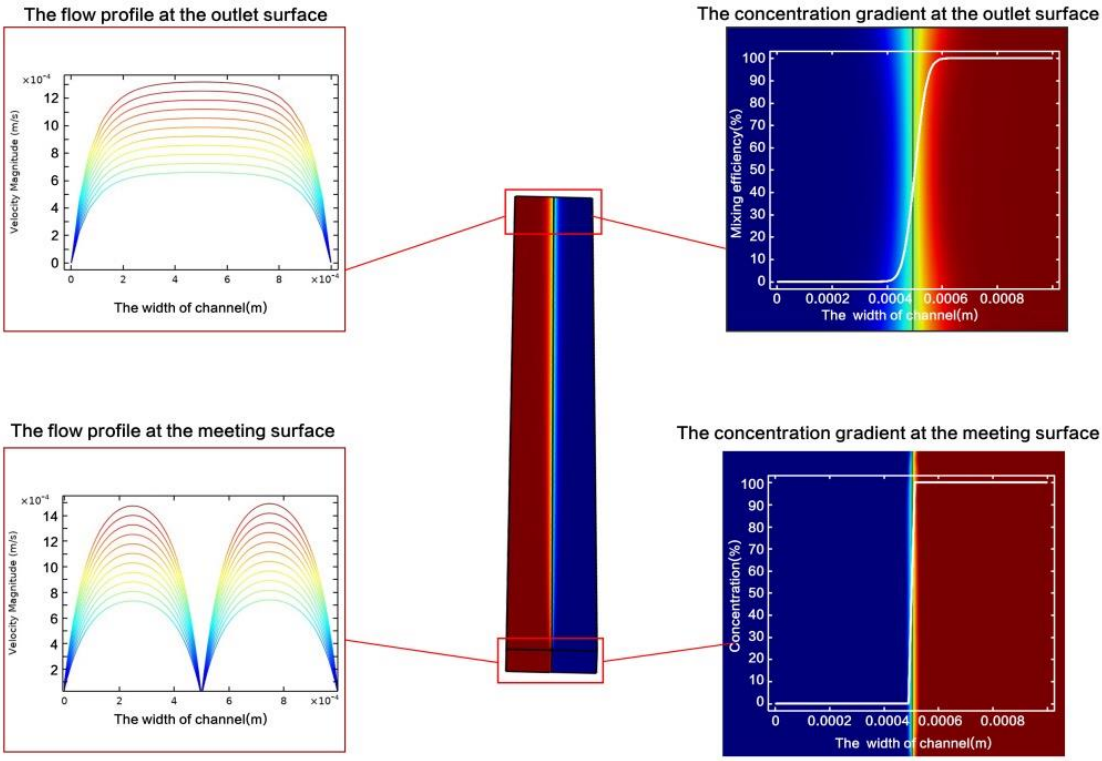

Figure 25. *The characteristics of flow and diffusion in the straight channel*

According to Figure 24 and Figure 25, the concentration gradients in two simulations at the 10 μl/min flow rate are seemingly similar. Thus, the detailed numerical data regarding mixing efficiency (ME) as the flow rate increases are presented in Table 1.

Table 1. *The comparison of mixing efficiency*

Flow rate (*μl/min*)	ME (%)_Straight	ME (%)_Integrated	Difference (%)
10	7.8930	7.8825	0.0105
11	7.5247	7.5147	0.0100
12	7.2035	7.1939	0.0096
13	6.9202	6.9109	0.0093
14	6.6678	6.6588	0.0090
15	6.4411	6.4324	0.0087
16	6.2360	6.2276	0.0084
17	6.0493	6.0411	0.0082
18	5.8785	5.8704	0.0081
19	5.7213	5.7134	0.0079
20	5.5761	5.5683	0.0078

In summary, the difference between the straight channel and the integrated geometry is as small as less than 0.01%. Thus, the hypothesis stands, and the results of a straight mixing channel can accurately reflect mixing efficiency on behalf of the integrated geometry. Furthermore, due to the validated hypothesis - the effect of supply channels on mixing efficiency is negligible. The shape optimization function is not necessary to be applied in the integrated geometry. The detailed mathematical relationship between the mixing efficiency and flow rate is discussed in Section 4.3.

4.2 Dimension optimization

On the previous simulation finding, the main subject to study can be simplified to be a straight mixing channel, instead of the integrated geometry, which dramatically increases the efficiency of computation load. Aim to further study the optimal dimension of the straight channel resulting in the minimum mixing efficiency, the optimization function built in the COMSOL® is employed. However, the types of dimensions to be optimized need

to be specified before the simulation. Briefly, the objective function, controllable variables, and constraints should be specified in the dimension optimization function. In this simulation, the objective function is specified as the mixing efficiency equation. The progress will automatically end till the minimization approximation to objective function appears, or the iteration reaches the maximum. The controllable variables regarding dimensions to a straight channel include three fundamental aspects, which are length, width, and height of a straight channel. Ideally, according to the diffusion equation discussed, the shorter length, the narrower width, the lower height result in smaller mixing efficiency. However, the observation area of the microfluidic chip prepared for biologists is limited in this thesis. The fixed monitoring area in the mixing channel is a rectangular area in which the length is 10 mm and the width is 1 mm. Only the height is the controllable variable input in the optimization node. Due to the height of most eukaryotic animal cells are around 10 μm [64] [65]. The range of height of channel controlled in the optimization is various from 50 μm to 300 μm in this thesis. Because the extremely low height of the channel, which is less than 50 μm, is likely to make cells uncomfortable. The geometry with a higher height requires a higher flow rate to reach a smaller mixing efficiency, which finally results in a large consumption of drug candidate. Thus, it is necessary to set up an upper bound and a lower bound to the dimension ‘height’.

One of the constraints is shear stress, which is less than 0.01 Pa. Considering the height of cells, the simulation results of shear stress are the maximum shear stress at the surface where is 5 μm above the bottom surface of the channel, as Figure 26 illustrates.

Furthermore, shear stress is a direct result of flow rate and fluid viscosity. Thus, the flow rate ranging from 1 μl/min to 15 μl/min is controlled as a variable in the process of dimension optimization.

Due to the optimization solver is a gradient-based solver, and the number of variables and constraints involved in this simulation is a handful. Thus, the process of simulation is relatively in the ease of computation. Table 2 illustrates the significant simulation results in each dimension, which fulfil the constraint while presenting the minimum mixing efficiency.

Table 2. *The primary optimization results in different dimensions*

Height (μm)	Flow rate (μl/min)	ME(%)	Shear stress (Pa)
300	14	6.6678	0.01051
250	10	7.2804	0.01069

200	6	8.5103	0.00988
150	4	9.1457	0.01047
100	2	10.714	0.01141
50	1	10.880	0.02248

These six optimum sets of results are selected from all optimization results, which present the best combination in each dimension. The step is set as 50 um for each. Only the set of ’50 μm’ does not show a valid result in the given range of flow rates. As the flow rate less than 1 μl/min is excluded from consideration in this thesis, so 50 μm height can be negligible. The 300 μm height associated with 14 μl/min displays the minimum mixing efficiency among six sets and meets the requirement of shear stress simultaneously.

Furthermore, when this set of parameters is considered in a conceptional platform’s perspective, the conclusion to the best choice is different. As the ideally maximum flow rate has clarified Section 3.4, the practical maximum flow is more likely to be 50% - 60% of the ideal one. Assume it is 50% of the ideal 16 μl/min, the practical flow rate in one minute will be 8 μl/min. Thus, the combination like 200 μm with 6 μl/min or 150 μm with 4 μl/min is more appropriate for the footprint case, depending on the shape of the reservoir and detailed layout.

4.3 Mathematical analysis

In the previous simulations, the geometry of channel, its dimensions, and the optimum flow rate are determined respectively based on some individual data from massive simulation data. In this section, all these data collected by utilizing dimension optimization function and parametric sweep function will be plotted and presented to clarify the mathematical relationships behind the data.

Firstly, two figures illustrating the status of mixing gradient and shear stress under the same flow rate in the straight mixing channel is presented below.

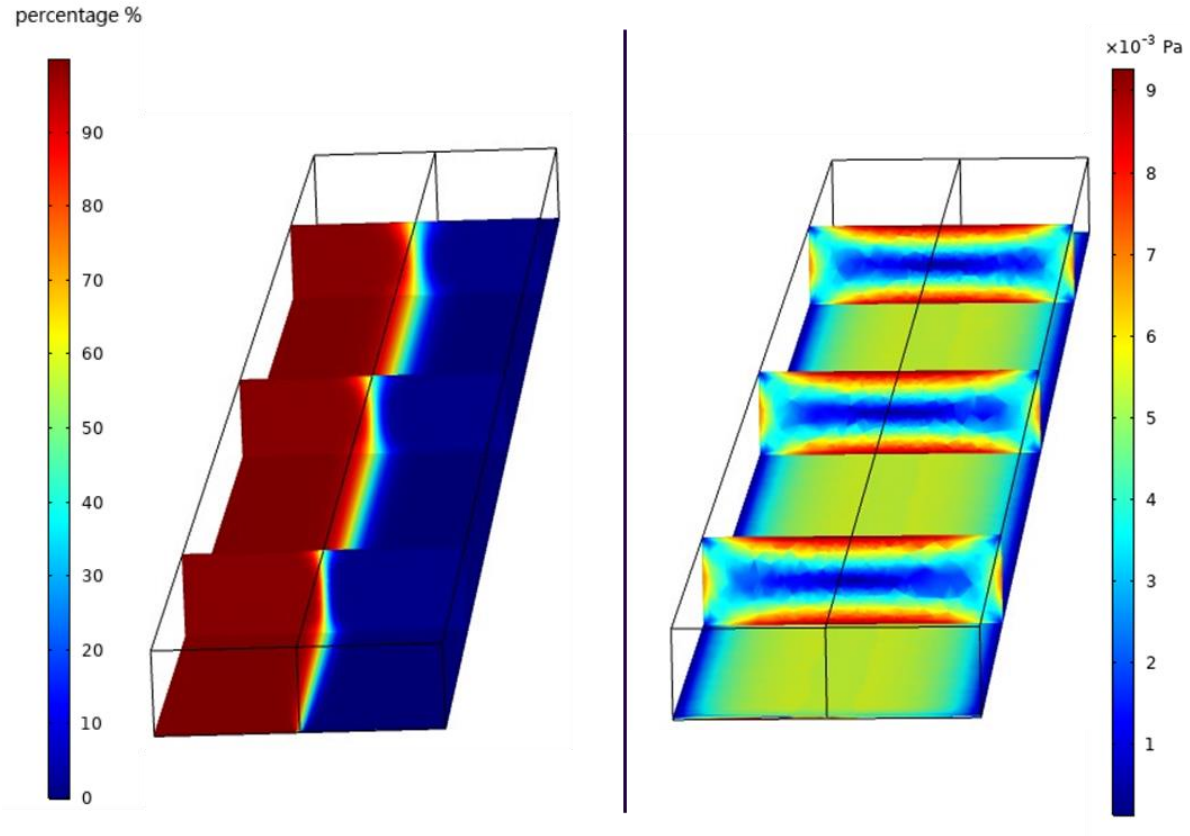

Figure 26. *The status of mixing efficiency (left) and shear stress (right)*

According to Figure 26, some equations related to mixing efficiency and shear stress can be illustrated visually. The degree of diffusion gradually increases along the length of the straight channel. Besides, its degree is not linear to the distance from the outlet, which can be interpreted by the diffusion equation. When it comes to the tendency of shear stress, the magnitudes of shear stress at the same horizontal cross profile approximately keep constant along the length of the channel. Whereas the magnitudes gradually increase when they are nearer the walls of the channel. Thus, the shear stress at the virtual line where is placed in the exact middle along the length of the channel may have the minimum value. In contrast, wall shear stress has maximum magnitude, except the corners.

In summary, the degree of diffusion is subjected to the length and the cross-section of the mixing channel. Whereas the magnitude of shear stress changes along with the height or the width of the channel.

Secondly, the data of mixing efficiency derived from a parametric sweep, which is specified a range for the flow rate (1-20 µl/min) and the height (50-300 µm), is plotted as below.

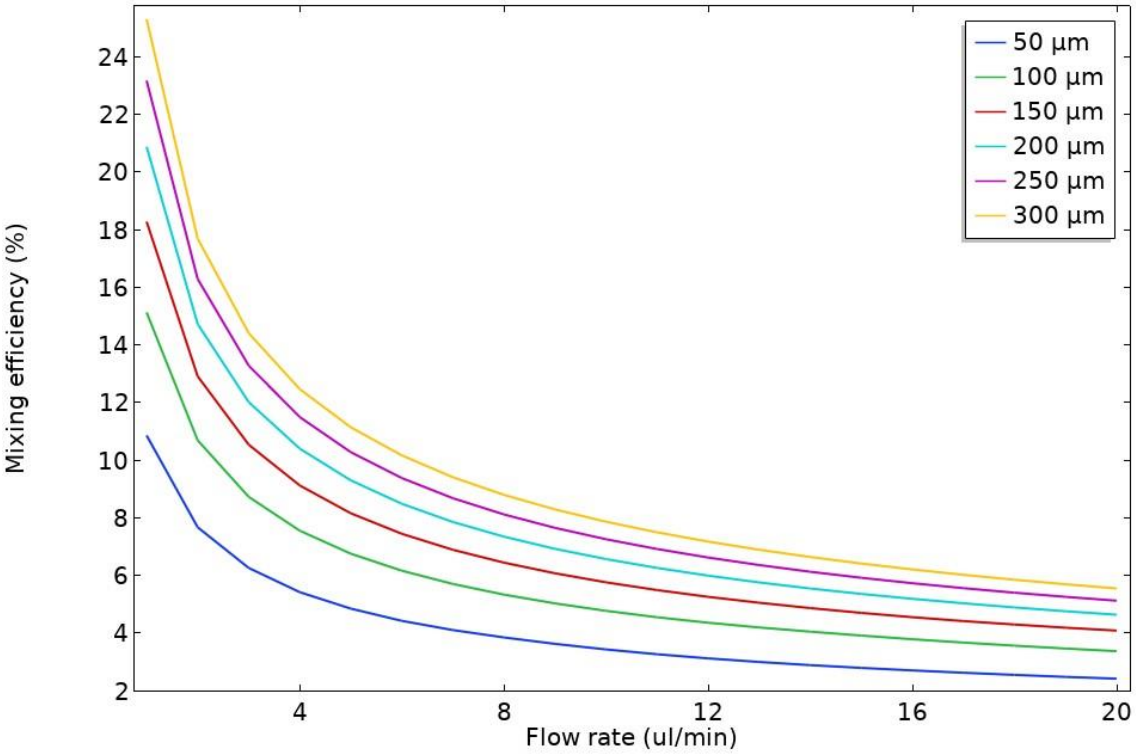

Figure 27. *The tendency of mixing efficiency in the different height of chip as flow rate changes, ranging from 50 µm height (blue line) to 300 µm (orange line)*

The curves ranging from the lowest blue one to the highest one represent the heights ranging from 50 µm to 300 µm correspondingly (see Figure 27). The *x*-axis refers to flow rate, and *y*-axis refers to mixing efficiency. Under the same flow rate magnitude, the lower height presents a lower mixing efficiency. The mixing efficiency does not have a linear relationship with flow rate, instead of a non-linear relationship expressed in a high order polynomial. The change rate of mixing efficiency is significant when the magnitude of flow rate is relatively small. Whereas the change rate does not change dramatically when the flow rate is big, for example, at 10 µl/min flow rate. According to all curves, in this case, applying a relatively large magnitude of flow rate is recommended, the reasons are to pursue a minimum mixing efficiency, and to improve the anti-disturbance characteristic of the microfluidic platform. In other words, a slight change in flow rate does not result in a considerable change in mixing efficiency.

In addition to the mathematical relationship between mixing efficiency and flow rate, the tendency of shear stress varying as the flow rate changes are also studied. Similar to the way of studying mixing efficiency, the data of shear stress is also derived from a parametric sweep, which is specified a range for the value of flow rate (1-20 µl/min) and the value of height (50-300 µm). Differently, the data of mixing efficiency is a global value that is collected by global evaluation function in the COMSOL ®, whereas the data of

shear stress is collected as the maximum value of shear stress at the surface where is 5 μm above the bottom of channel (see Figure 26).

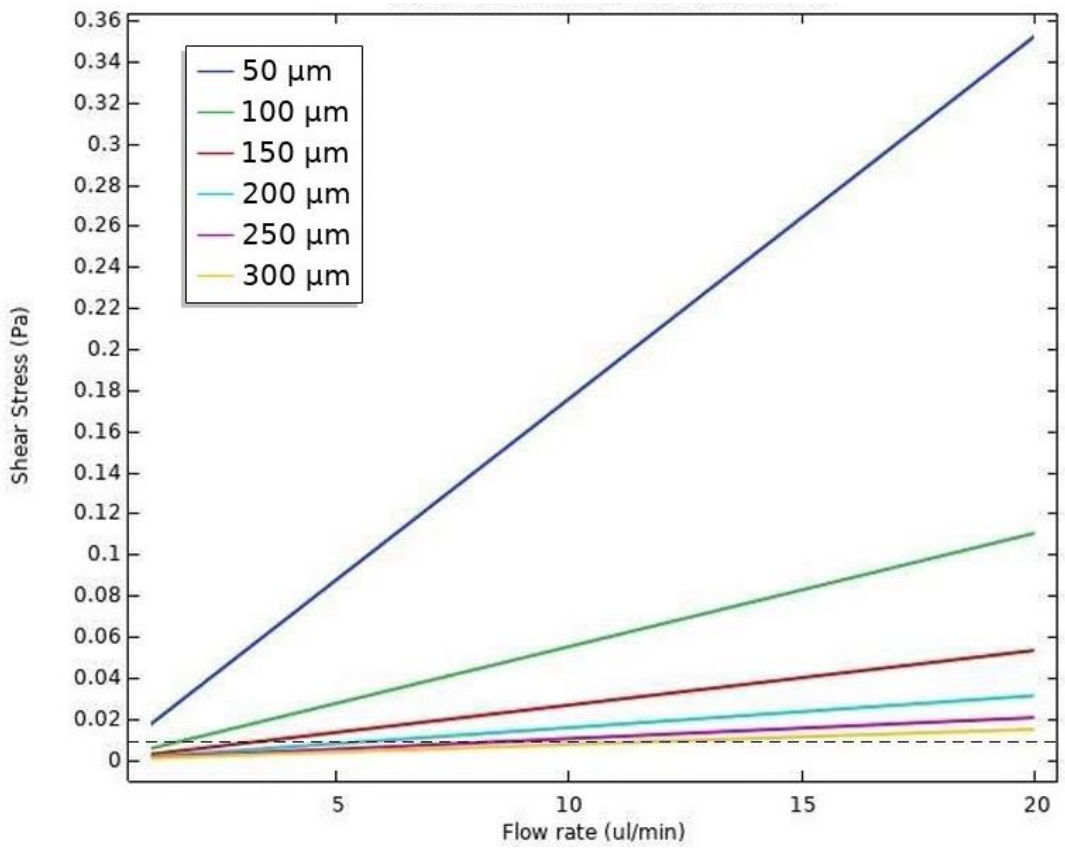

Figure 28. *The tendency of shear stress in the different height of chip as flow rate changes, ranging from 50 μm (blue line) to 300 μm (orange line)*

The curves from top to bottom represent the height ranging from 50 μm to 300 μm correspondingly (see Figure 28). The shear stress has a linear relationship with flow rate. This tendency is consistent with the mathematical equations of shear stress, which merely involves shear rate and fluid viscosity. The slope of curves from top to bottom presents a dropping tendency. Notably, the rate of dropping is gradually slow, which benefits the selection of a proper height of geometry. According to the limit magnitude of shear stress - 0.01 Pa (dotted line in Figure 28), the 50 μm and 100 μm selections are excluded. Because both these selections only match the requirement of shear stress when the flow rate is relatively low, which is not consistent with the practical objective. Furthermore, within the rest four selections, the mixing efficiency and its corresponding shear stress are compared in sequence at the same magnitude of flow rate. Finally, 'the 200 μm height with 6 μl/min', this combination shows its competitivity above others.

4.4 Validations of the microfluidic chip

The validations experiments are implemented by two microfluidic platforms, the syringe-based one, and the pressure-based one. The main parameters applied in two platforms are as identical to those in the simulations possible. The syringe-based experiment aims to visually validate the feasibility of implementing experimental objectives (see Figure 29). In comparison to the pressured-based experiments, the syringed-based platform characterizes easy implementation, experimental results by visual. However, as the food colour solutions pumped in the chips are the mixtures in which their diffusion coefficients are unknown. Thus, the comparison between the mixing gradient generated in the straight channel and that of in the simulations is meaningless.

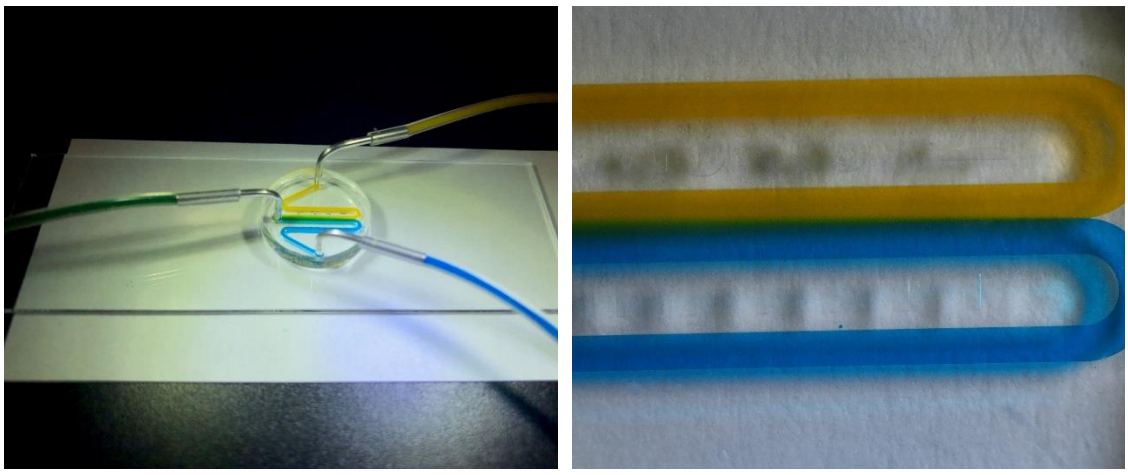

Figure 29. *A chip tested with food colour solutions*

Although the syringe-based platform shows a series of merits, the limited size of syringes confines its potential applying in a long-term experiment. Thus, the pressure-based platform was proposed and then used in the final validation experiments.

The validation results by employing the pressure-based pump and FITC solution are presented below (see Figure 30). The images are shown in black (buffer solutions) and green colours (FITC) under the fluorescence microscope. Under the constant 6 μl/min flow rate, the distribution of FITC at 1 mm after the junction, and at 9 mm after the junction under the microscope.

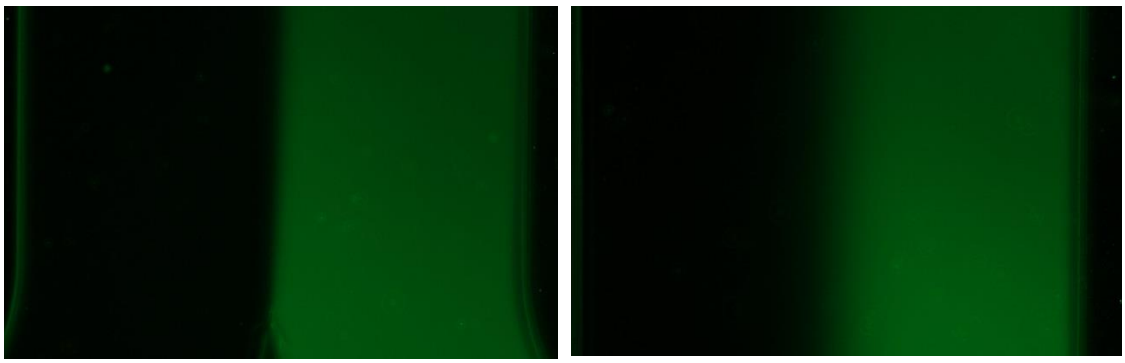

Figure 30. *The distribution of FITC at 1 mm (left) and 9 mm (right) after the junction under the microscope*

Visually, the dividing line, which is supposed to be squarely in the middle, tends to be a right skew in two figures. Theoretically, when two flow meets at the junction having the same magnitude of flow rate and identical viscosity, the dividing line will divide the width of the channel in half accurately. Otherwise, the dividing line trends to skew the side of having a small flow rate and small viscosity. As FITC's concentration is only 1 mM in this thesis, the difference between two solutions in terms of viscosity can be negligible. The main reason resulting in this consequence is the difference in flow rate. Different from the way of regulating flow rate by a step motor in the syringe pump, the pressure-based platform depends on the hydraulic resistances. The hydraulic resistance varies because of mechanical or manual cuts. According to the hydraulic resistance equation discussed in Section 3.5.2, the characteristic length and diameter determine the magnitude of resistance. In this experiment, as the desired flow rate is 6 µl/min, so the diameters of the selected resistor are relatively small, which are 30 µm, 50 µm, or 63 µm. Besides, if the lengths of all resistors are confined in a range of 20 mm to 50 mm, the resistors will be convenient to handle by laboratory technician. Thus, even a small tolerance of resistance generated by manually cutting may result in an unbalance flow rate in the experiments. Furthermore, the impurities and FITC particles within the flow may also cause a possibility of blocking tubing.

In addition to dividing line, the intensity of FITC along the channel is worth to pay an attention. At 1 mm after the junction, the intensity is obviously stronger than that of at 9 mm after the junction. The FITC molecules horizontally diffuse to the other side along the length of channel based on the diffusion effect. It is not hard to understand that the intensity of FITC becomes mild in the end.

In order to convert the images of diffusion profile to numerical data, Figure 31 is measured by an image analysing tool, ImageJ. Figure 31 illustrates the comparison regarding the diffusion profile between experimental validation and simulation.

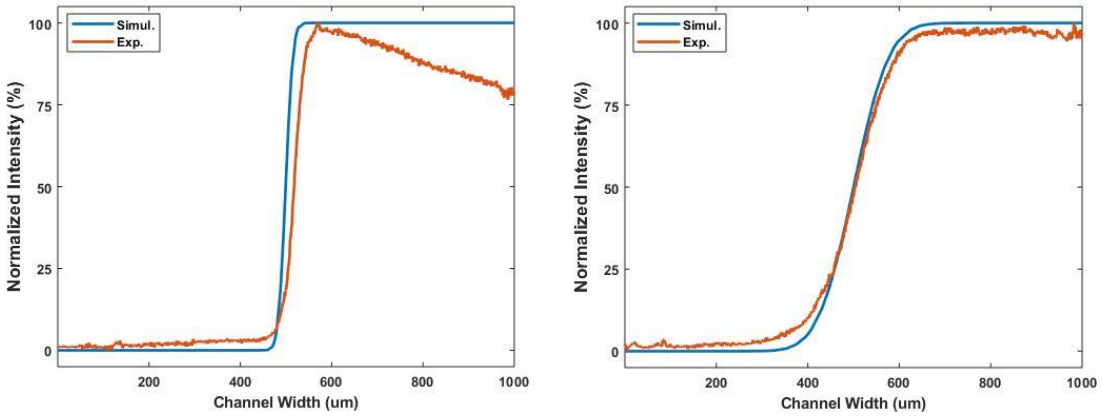

Figure 31. *Experimental validation of cross-sectional diffusion profiles (red lines), which were compared with theoretical simulations (blue lines) at 1 mm (left) and 9 mm (right) after the junction*

The curves of validation properly match those of simulation. However, there are still some defects in the experimental curves that need to be noticed, such as they are not as smooth as simulation counterparts, and the magnitude of mixing efficiency is slightly bigger than simulation ones. Mainly, for the part where is at 1 mm below the junction, the intensity does not keep constant in 100% on the side of FITC, instead of displaying a downward trend. There are some explains that may clarify this outcome. The most convincing one is the uneven height of the channel, resulting in an unbalance focus of the camera lens cause an uneven intensity of FITC finally in the images. Besides, the uneven height is a direct result of an unsatisfied spinning coating on the wafer substrate. More experiments and validations are needed to make this consequence clear. In summary, the experimental data is approximately consistent with the simulation data.

4.5 Discussion

In this section, some insufficiencies of the microfluidic platforms, and some unexpected situations appearing during the experimental validations are discussed, trying to alleviate or even eliminate them in the future.

Firstly, the setup of simulations has limitations to some extent, ranging from the design of microfluidic chip to the selection of parameters. The current design of chip matches the current biomedical objectives sufficiently. However, if the biologists ask a fully-developed chemotactic gradient at the same time, this design is not appropriate. Thus, in the subsequent experiments, a new geometry is recommended to be designed, which can match two different objectives. Speaking of the selection of parameters, as the solute applied in the experiments is solely FITC, only one diffusion coefficient of FITC is considered. However, for a real biological experiment that involves two or more solutes, the

diffusion may happen in a bidirectional or a multidirectional way. One solute has a different diffusion coefficient in a different solution. The setup in the transport diluted species interface in the COMSOL® will be complicated.

Secondly, the uneven height of SU-8 mold fabricated in the course of spin-coating need to be improved. The uneven height has a significant impact on the accuracy of image analyse. As the curves of diffusion profile discussed before (see Figure 31), it results to a descending trend. In the next microfabrication, the quality of spin-coating needs to be better and the distribution of height is more uniform. Furthermore, if the pattern of each chip is numbered in the process of designing SU-8 mold, and each chip's distribution of height is measured after fabrication, the risk of using defective chips will be eliminated.

Thirdly, the slight difference in the length of a hydraulic resistor may lead to a huge difference in flow rate, if the diameter of the resistor is small enough. Furthermore, too long or too short resistor handled in the experiments may cause inconvenience to laboratory technician. Thus, in the subsequent experiments, a more standardized and rigorous operation are needed.

Finally, the most significantly unexpected situation appears in the experiments is bubble generation. The bubbles are 'fatal' to cells in a flow experiment. In general, the observation area to cells will lost some adhered cells after one bubble goes through. The bubbles can generate in the course of manually filling syringes. Furthermore, the temperature gradient along the perfusion tubing promotes the generation of air bubbles. The physical principle explaining this effect is the solubility of gas in liquids. At higher temperature, water can absorb less gas than at lower temperatures. In the current experiments, the temperature is maintained at 37℃ merely for chips, instead of tubing. The medium is prepared in the room temperature or is keep in the fridges. Thus, it is inevitable that a temperature gradient will generate along with the tubing.

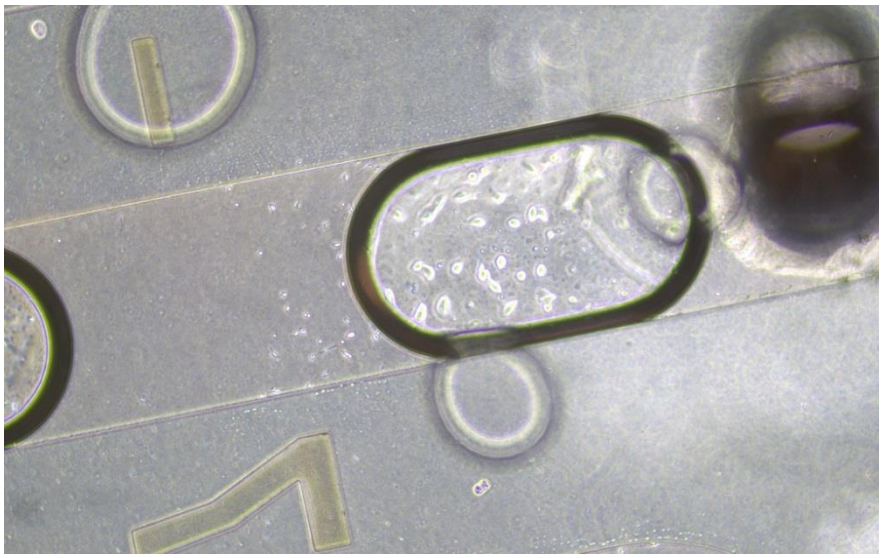

Figure 32. *A bubble damages the adhered cells*

In order to reduce the formation of gas bubbles in the later experiments, some methods are useful. The first method is to eliminate the difference in temperature between chips and tubing by pre-heating the solutions and the tubing before utilizing. Another way is to assemble a bubble trap at the end of tubing to catch bubbles before they flow into the chips. Some classic bubble traps exist over the years [66] [67]. Furthermore, depending on the period of experiment, to shorten the experimental time favours the elimination of bubble generation. The details of bubble trap will not be discussed here.

In the experiments to come, the improvements will be implemented one by one resulting in a versatile and stable microfluidic platform.

5. CONCLUSION

This thesis contributes to theoretically illustrating the integrated process of studying the microfluidic chip in a concise and comprehensive way, starting from design and ending to experimental validations. The design of microfluidic chip as one of the main themes in this thesis, aims to generate a desired chemotactic gradient to guide the chemotactic movement of cancer cells. The original principle of the design derives from the model of classic laminar micromixers in which the mixing efficiency is relatively small in comparison to active micromixers. The geometry of micromixer is further refined by utilizing the function of dimensional optimization in the COMSOL®. However, the judgement and decision to the ultimate geometry are not only determined by simulation results, but also is limited by shear stress (0.01 Pa), and the fixed-sized of the conceptional platform. Furthermore, the simulation results are validated by two microfluidic platforms, which are syringed-based one and pressure-based one. The syringed-based platform is assigned to validate the feasibility of this thesis, and the pressure-based platform contributes to validating the accuracy of simulation results regarding mixing efficiency in comparison to experimental counterparts.

In conclusion, the experimental results are sufficiently consistent to the simulation counterparts. The pressure-based platform enables users to regulate the magnitude of flow rate accurately and to acquire an expected chemotactic gradient. However, in the case of the experiments involving cancer cells, the results are susceptible and unsatisfactory becasue the massive bubbles emerge. In the subsequent experiments to come, the flaws in relation to bubbles, and resistances will be mitigated as the gradual improvement of the microfluidic platform.

REFERENCES

[1] G. K. Stylios, "There is plenty of room at the bottom, R.P. Feynman," International Journal of Clothing Science and Technology, vol. 25, (5), pp. 336-337, 2013.

[2] XIA, Y. and WHITESIDES, G.M., 1998. Soft Lithography. Angewandte Chemie International Edition, 37(5), pp. 550-575.

[3] M. A. Unger et al, "Monolithic Microfabricated Valves and Pumps by Multilayer Soft Lithography," Science, vol. 288, (5463), pp. 113-116, 2000.

[4] HONG, X., JIANG, F., KALKANIS, S.N., ZHANG, Z.G., ZHANG, X., ZHENG, X., JIANG, H., MIKKELSEN, T. and CHOPP, M., 2008. Increased chemotactic migration and growth in heparanase-overexpressing human U251n glioma cells. Journal of experimental & clinical cancer research : CR, 27(1), pp. 23.

[5] LOURENCO, S., TEIXEIRA, V.H., KALBER, T., JOSE, R.J., FLOTO, R.A. and JANES, S.M., 2015. Macrophage migration inhibitory factor-CXCR4 is the dominant chemotactic axis in human mesenchymal stem cell recruitment to tumors. Journal of immunology (Baltimore, Md.: 1950), 194(7), pp. 3463-3474.

[6] GHALLAB, Y.H., BADAWY, W. and EBRARY, I., 2010. Lab-on-a-chip: techniques, circuits, and biomedical applications. Norwood, MA: Artech House

[7] JONES, G. and KRAFT, A., 2004. Corporate venturing: the origins of Unilever's pregnancy test. Business History, 46(1), pp. 100-122

[8] TANNENBAUM, J. and BENNETT, B.T., 2015. Russell and Burch's 3Rs then and now: the need for clarity in definition and purpose. Journal of the American Association for Laboratory Animal Science : JAALAS, 54(2), pp. 120-132.

[9] CHANG, C., CHENG, Y., TU, M., CHEN, Y., PENG, C., LIAO, W. and TUNG, Y., 2014. A polydimethylsiloxane-polycarbonate hybrid microfluidic device capable of generating perpendicular chemical and oxygen gradients for cell culture studiesElectronic supplementary information (ESI) available. See DOI: 10.1039/c4lc00732h. 14(19), pp. 3762-3772

[10] CAPRETTINI, V., CEREA, A., MELLE, G., LOVATO, L., CAPOZZA, R., HUANG, J., TANTUSSI, F., DIPALO, M. and DE ANGELIS, F., 2017. Soft electroporation for delivering molecules into tightly adherent mammalian cells through 3D hollow nanoelectrodes. Scientific reports, 7(1), pp. 8524-8.

[11] SITTINGER, M., SCHULTZ, O., KEYSZER, G., MINUTH, W.W. and BURMESTER, G.R., 1997. Artificial tissues in perfusion culture. The International journal of artificial organs, 20(1), pp. 57.

[12] Anonymous "Microfluidics Market By Materials (Polymers, Silicon, Glass), Pharmaceuticals (Microreactors, Toxicity Screening, Lab on Chip, Proteomic & Genomic Analysis) Drug Delivery Devices (Microneedles, Micropumps), IVD (POC) - Global Trends & Forecast to 2018," PR Newswire, 2013.

[13] LI, C., CHEN, R. and YANG, M., 2007. Generation of linear and non-linear concentration gradients along microfluidic channel by microtunnel controlled stepwise addition of sample solution. Lab on a chip, 7(10), pp. 1371.

[14] SELIMOVIĆ, Š, SIM, W.Y., KIM, S.B., JANG, Y.H., LEE, W.G., KHABIRY, M., BAE, H., JAMBOVANE, S., HONG, J.W. and KHADEMHOSSEINI, A., 2011. Generating Non-Linear Concentration Gradients in Microfluidic Devices for Cell Studies. Analytical Chemistry, 83(6), pp. 2020-2028.

[15] RICHARDS, G.R., MILLARD, R.M., LEVERIDGE, M., KERBY, J. and SIMPSON, P.B., 2004. Quantitative assays of chemotaxis and chemokinesis for human neural cells. Assay and drug development technologies, 2(5), pp. 465-472.

[16] BAGGIOLINI, M., 2001. Chemokines in pathology and medicine. Journal of internal medicine, 250(2), pp. 91-104.

[17] DHAWAN, P. and RICHMOND, A., 2002. Role of CXCL1 in tumorigenesis of melanoma. Journal of leukocyte biology, 72(1), pp. 9.

[18] MEIER, B., ZIELINSKI, A., WEBER, C., ARCIZET, D., YOUSSEF, S., FRANOSCH, T., RÄDLER, J.O. and HEINRICH, D., 2011. Chemotactic cell trapping in controlled alternating gradient fields. Proceedings of the National Academy of Sciences of the United States of America, 108(28), pp. 11417-11422.

[19] HADDOX, J.L., KNOWLES, I.W., SOMMERS, C.I. and PFISTER, R.R., 1994a. Characterization of chemical gradients in the collagen gel-visual chemotactic assay. Journal of immunological methods, 171(1), pp. 1.

[20] JOHN, T.J. and SIEBER, J.,O F., 1976. Chemotactic migration of neutrophils under agarose. Life Sciences, 18(2), pp. 177.

[21] NELSON, R.D., QUIE, P.G. and SIMMONS, R.L., 1975. Chemotaxis Under Agarose: A New and Simple Method for Measuring Chemotaxis and Spontaneous Migration of Human Polymorphonuclear Leukocytes and Monocytes. The Journal of Immunology, 115(6), pp. 1650.

[22] ZICHA, D., DUNN, G.A. and BROWN, A.F., 1991. A new direct-viewing chemotaxis chamber. Journal of cell science, 99 (Pt 4), pp. 769.

[23] ZIGMOND, S.H., 1977. Ability of Polymorphonuclear Leukocytes to Orient in Gradients of Chemotactic Factors. The Journal of cell biology, 75(2), pp. 606-616.

[24] DERTINGER, S.K.W., CHIU, D.T., JEON, N.L. and WHITESIDES, G.M., 2001. Generation of Gradients Having Complex Shapes Using Microfluidic Networks. Analytical Chemistry, 73(6), pp. 1240-1246.

[25] KALLIO, P. and KUNCOVA, J., 2004. Microfluidics. Helsinki: Tekes.

[26] WU, M., HUANG, S. and LEE, G., 2010. Microfluidic cell culture systems for drug research. Lab on a chip, 10(8), pp. 939.

[27] ARTICLE, J., 2007. Application of LBM in Simulation of Flow in Simple Micro-Geometries and Micro Porous Media.

[28] PAUL, O.B., 2015. Evaluation of mixing efficiency in a microfluidic cartridge using a finite element method approach. Tampere University.

[29] Peclet number. 2009. 2 edn. Oxford University Press

[30] A Novel Method of Constructing an Electroosmotic Micromixer with Double-Side Electrodes for Biotechnological Applications. 2015. Sensors and Materials, pp. 1

[31] CAI, G., XUE, L., ZHANG, H. and LIN, J., 2017. A Review on Micromixers. Micromachines, 8(9), pp. 274.

[32] HESSEL, V., LÖWE, H. and SCHÖNFELD, F., 2005. Micromixers—a review on passive and active mixing principles. Chemical Engineering Science, 60(8), pp. 2479-2501.

[33] CHENG, Y., JIANG, Y. and WANG, W., 2018. Numerical simulation for electroosmotic mixing under three types of periodic potentials in a T-shaped micromixer. Chemical Engineering and Processing - Process Intensification, 127, pp. 93-102.

[34] CHEN, H. and HU, Y., 2006. Bioreactors for tissue engineering. Biotechnology Letters, 28(18), pp. 1415-1423.

[35] JAASMA, M.J. and O'BRIEN, F.J., 2008. Mechanical stimulation of osteoblasts using steady and dynamic fluid flow. Tissue engineering. Part A, 14(7), pp. 1213-1223.

[36] GERHART, P.M., GERHART, A., L., HOCHSTEIN, J.I., MUNSON, B.R., YOUNG, D.F. and OKIISHI, T.H., 2016. Munson, Young and Okiishi's fundamentals of fluid mechanics. 8th edn. Hoboken: Wiley.

[37] HAYT, W.H.,Jr and KEMMERLY, J.E., 1993. Engineering circuit analysis. 5th, international edn. New York: McGraw-Hill.

[38] SJODIN, B., 2016. What's The Difference Between FEM, FDM, and FVM? Machine Design.

[39] NAKASONE, Y., STOLARSKI, T. and YOSHIMOTO, S., 2018. Engineering Analysis with ANSYS Software, 2nd Edition. Butterworth-Heinemann.

[40] TABATABAIAN, M. and BOOKS24X7, I., 2014. COMSOL for engineers. Dulles, VA: Mercury Learning and Information.

[41] WALTER, F., 2016. Keeping Track of Element Order in Multiphysics Models. Comsol, USA. [viewed 04/05/2019]. Available from: https://www.comsol.fi/blogs/keeping-track-of-element-order-in-multiphysics-models/

[42] JEONG, W. and SEONG, J., 2014. Comparison of effects on technical variances of computational fluid dynamics (CFD) software based on finite element and finite volume methods. International Journal of Mechanical Sciences, 78, pp. 19-26

[43] GRADIENTECH., 2016. Chemotaxis towards stable gradients. [viewed 15/02/2019]. Available from: https://gradientech.se/celldirector/2d/

[44] DONG, L., CHEN, D., LIU, S. and DU, W., 2016. Automated Chemotactic Sorting and Single-cell Cultivation of Microbes using Droplet Microfluidics. Scientific reports, 6(1), pp. 24192.

[45] KREUTZER, J., HONKANEN, M., LAAKSONEN, J. and KALLIO, P., 2010. Perfusion characterization using flow simulations and μPIV measurements.

[46] BABENDREYER, A., MOLLS, L., DREYMUELLER, D., UHLIG, S. and LUDWIG, A., 2017. Shear Stress Counteracts Endothelial CX3CL1 Induction and Monocytic Cell Adhesion. Mediators of inflammation, 2017, pp. 1515389-10.

[47] MA, S., FU, A., LIM, S., CHIEW, G.G.Y. and LUO, K.Q., 2018. MnSOD mediates shear stress-promoted tumor cell migration and adhesion. Free Radical Biology and Medicine, 129, pp. 46-58.

[48] YAN, W.W., CAI, B., LIU, Y. and FU, B.M., 2012. Effects of wall shear stress and its gradient on tumor cell adhesion in curved microvessels. Biomechanics and Modeling in Mechanobiology, 11(5), pp. 641-653.

[49] ABGRALL, P., CONEDERA, V., CAMON, H., GUE, A. and NGUYEN, N., 2007. SU‐8 as a structural material for labs‐on‐chips and microelectromechanical systems. Electrophoresis, 28(24), pp. 4539-4551.

[50] ZHANG, J., TAN, K.L. and GONG, H.Q., 2001. Characterization of the polymerization of SU-8 photoresist and its applications in micro-electro-mechanical systems (MEMS). Polymer Testing, 20(6), pp. 693-701.

[51] POTRICH, C., LUNELLI, L., COCUZZA, M., MARASSO, S.L., PIRRI, C.F. and PEDERZOLLI, C., 2019. Simple PDMS microdevice for biomedical applications. Talanta, 193, pp. 44-50.

[52] ALMUTAIRI, Z., REN, C.L. and SIMON, L., 2012. Evaluation of polydimethylsiloxane (PDMS) surface modification approaches for microfluidic applications. Colloids and Surfaces A: Physicochemical and Engineering Aspects, 415, pp. 406-412.

[53] DIENER., 2016. Plasma systems. [viewed 02/04/2019]. Available from: https://www.plasma.com/en/produkte/plasmaanlagen/niederdruckplasmaanlagen/pico/

[54] BHATTACHARYA, S., DATTA, A., BERG, J.M. and GANGOPADHYAY, S., 2005. Studies on surface wettability of poly(dimethyl) siloxane (PDMS) and glass under oxygen-plasma treatment and correlation with bond strength. Journal of Microelectromechanical Systems, 14(3), pp. 590-597.

[55] BHATTACHARYA, S., DATTA, A., BERG, J.M. and GANGOPADHYAY, S., 2005. Studies on surface wettability of poly(dimethyl) siloxane (PDMS) and glass under oxygen-plasma treatment and correlation with bond strength. Journal of Microelectromechanical Systems, 14(3), pp. 590-597.

[56] WANG, L., SUN, B., ZIEMER, K.S., BARABINO, G.A. and CARRIER, R.L., 2009. Chemical and physical modifications to poly(dimethylsiloxane) surfaces affect adhesion of Caco ‐ 2 cells. Journal of Biomedical Materials Research Part A, 93A(4), pp. 1260-1271.

[57] HEMMILÄ, S., CAUICH-RODRÍGUEZ, J.V., KREUTZER, J. and KALLIO, P., 2012. Rapid, simple, and cost-effective treatments to achieve long-term hydrophilic PDMS surfaces. Applied Surface Science, 258(24), pp. 9864-9875.

[58] BYUN, C.K., ABI ‐ SAMRA, K., CHO, Y. and TAKAYAMA, S., 2014. Pumps for microfluidic cell culture. Electrophoresis, 35(2-3), pp. 245-257.

[59] MÄKI, A.-., PELTOKANGAS, M., KREUTZER, J., AUVINEN, S. and KALLIO, P., 2015. Modeling carbon dioxide transport in PDMS-based microfluidic cell culture devices. Chemical Engineering Science, 137, pp. 515-524

[60] BLAU, A., NEUMANN, T., ZIEGLER, C. and BENFENATI, F., 2009. Replica-moulded polydimethylsiloxane culture vessel lids attenuate osmotic drift in long-term cell cultures. Journal of Biosciences, 34(1), pp. 59-69.

[61] OKOLAB., 2016. H601-K-FRAME-GLASS-FLAT. [viewed 16/07/2019]. Available from: http://www.oko-lab.com/ivf/heating-devices-ivf/others/h601-k-frame-glass-flat-other

[62] ZEISS,. 2016. ZEISS Axio Observer for Biology. [viewed 20/07/2019]. Available from: https://www.zeiss.com/microscopy/int/products/light-microscopes/axio-observer-for-biology.html

[63] FITC. 2010. 1 edn. Oxford University Press.

[64] JUNQUEIRA, L.C. and CARNEIRO, J., 2003. Basic histology: text and atlas. 10. edn. New York: Lange Medical Books/McGraw-Hill, Medical Publishing Division.

[65] VICKARYOUS, M.K. and HALL, B.K., 2006. Human cell type diversity, evolution, development, and classification with special reference to cells derived from the neural crest. Biological Reviews, 81(3), pp. 425-455.

[66] CHENG, D. and JIANG, H., 2009. A debubbler for microfluidics utilizing air-liquid interfaces. Applied Physics Letters, 95(21), pp. 21410-3.

[67] STUCKI, J.D. and GUENAT, O.T., 2015. A microfluidic bubble trap and oscillator. Lab on a chip, 15(23), pp. 4393-4397.